

Low-rank tensor decompositions of quantum circuits

Quantum computing is arguably one of the most revolutionary and disruptive technologies of this century. Due to the ever-increasing number of potential applications as well as the continuing rise in complexity, the development, simulation, optimization, and physical realization of quantum circuits is of utmost importance for designing novel algorithms. We show how matrix product states (MPSs) and matrix product operators (MPOs) can be used to express not only the state of the system but also quantum gates and entire quantum circuits as low-rank tensors. This allows us to analyze and simulate complex quantum circuits on classical computers and to gain insight into the underlying structure of the system. We present different examples to demonstrate the advantages of MPO formulations and provide a new perspective on the construction of quantum algorithms.

Keywords: quantum computing, quantum simulation, matrix product states, matrix product operators, tensor trains

MSC: 15A69, 47N50, 65C05, 68W40, 81P68

Patrick Gelß

AI in Society, Science, and Technology, Zuse Institute Berlin, Berlin 14195, Germany

Department of Mathematics and Computer Science, Freie Universität Berlin, Berlin 14195, Germany

Stefan Klus

Department of Mathematics, University of Surrey, Guildford GU2 7XH, UK

Zarin Shakibaei

Telekom Innovation Laboratories, Technische Universität Berlin, Berlin 10623, Germany

Sebastian Pokutta

AI in Society, Science, and Technology, Zuse Institute Berlin, Berlin 14195, Germany

Institute of Mathematics, Technische Universität Berlin, Berlin 10623, Germany

1 Introduction

Over the last decades, the interest in *quantum computing*—both the theory and physical realization of qubits and quantum algorithms—has increased significantly. Especially since Google [1] claimed in 2019 to have reached *quantum supremacy*, i.e., the point at which a quantum computer outperforms classical computers by solving problems that are known to be intractable for conventional computers, quantum computing has attracted widespread scientific and public attention. Quantum computing exploits quantum-mechanical effects such as quantum entanglement and superpositions of quantum states. Instead of storing information in the form of bits that can be either in state 0 or 1, a quantum computer uses *qubits* that can represent both states simultaneously. In 1981/1982, Richard Feynman proposed the concept of quantum computing [2], based on *quantum logic gates*, i.e., unitary operations acting on a quantum register, which led to a paradigm shift. Subsequent breakthroughs in the history of quantum computing include *Shor's algorithm* for factoring integers [3], *Grover's algorithm* for searching unsorted databases [4], and *Simon's algorithm* for finding periods of functions [5]. The first two of these algorithms exhibit a (super-)polynomial and the latter an exponential speed-up in comparison to the best known classical algorithms.

Since the full potential of quantum parallelism is now evident and quantum computers become a reality, this new technology has been considered with increasing frequency in various application areas such as finance [6, 7], cryptography [8, 9], chemistry [10, 11], and machine learning [12, 13]. Moreover, different computer architectures have been considered over the last years, see, e.g., [14–17], and particularly superconducting quantum computing [18] is realized by various companies such as IBM, Google, and Intel. Despite recent advances, however, increasing the number of qubits of quantum computers as well as developing new quantum algorithms remain complex challenges. Discoveries of algorithms that are able to solve real-world problems and, at the same time, outperform known classical algorithms have been scarce in the past years. From a theoretical point of view, different techniques such as genetic programming [19] or quantum walks [20] have shown to be potential frameworks for discovering new quantum algorithms. Developing new algorithms requires concepts and tools that are able to express the logic behind complex quantum circuits and translate classical mathematical operations into instructions that can be executed on quantum computers and vice versa.

Due to its significance for understanding the computational benefits and developing new algorithms, the numerical simulation of quantum computers on classical hardware is of utmost importance. Quantum simulation can help us to explore the opportunities and limitations of quantum computers, although it typically leads to highly complex numerical problems since typically the storage consumption and the computational costs grow exponentially with the number of qubits. This is also referred to as the *curse of dimensionality*. There is a need for improved techniques for constructing and simulating complex quantum systems.

One approach to tackle such high-dimensional quantum states and circuits is to represent them in the form of tensor networks. Various methods based on *matrix product states* [21–25], *projected entangled pair states* (PEPS) [26], and the *multi-scale entanglement renormalization ansatz* (MERA) [27] have been proposed for enhancing quantum simulations. In this work, we will focus on qubit systems coupled in a one-dimensional fashion and the representation of quantum states in MPS format, which enables us to significantly reduce the numerical complexity if the underlying entanglement structure allows for low-rank decompositions. In fact, MPS decompositions were already introduced in the context of quantum physics in 1987 [28] and reinvented in applied mathematics around 2009 under the name *tensor trains* (TT), see [29, 30]. Tensor trains have become a widely-studied concept, which—besides the application in quantum mechanics, see, e.g., [31, 32]—found its way into other scientific fields such as the analysis of dynamical systems [33], system identification [34], and also quantum machine learning [35]. Different efficient algorithms have been developed, ranging from least-squares solvers to data-driven methods, e.g., SALSA [36], ARR [37], MANDy [38], AMUSEt [39], and tgEDMD [40]. Moreover, the tensor formalism allows for compact expressions, systematic decompositions, and direct analysis of the entanglement of quantum states as we will show below.

As mentioned above, the MPS format has been utilized in the context of quantum circuits before. However, mostly tensor decompositions of quantum states were considered thus far. The aim of this work is to represent not only quantum states but also quantum gates and entire circuits in the form of tensor networks by using *matrix product operators*, a natural extension of MPS tensors. MPO representations of quantum circuits indeed have been exploited recently [41, 42], but only by means of one- and two-qubit operators satisfying the nearest-neighbor constraint [43] with no focus on closed expressions or systematic decompositions. Analogously to the representation of quantum states in MPS format, we want to derive low-rank MPO representations for (networks of) quantum gates acting on arbitrary qubits within the register. We examine several quantum circuits by contracting MPS and MPO networks so that the probability distribution can either be constructed directly as a tensor or efficiently sampled by using a generative sampling strategy [44, 45]. Although quantum states, gates, and even circuits have been analyzed in terms of the MPS and MPO format in numerous publications, extensive studies of explicit MPO representations of complex quantum circuits have, to our knowledge, not been considered before. Our goal is not only to show how to use the MPS/MPO formalism to gain insight into the network structure of quantum systems, but also to open up new avenues for tensor-based research, in particular pertaining to the development of quantum algorithms. The techniques proposed in this paper introduce a new framework for designing and simulating complex quantum circuits as they provide access to them via closed-form operator representations. We show that various circuits can be expressed as weakly entangled MPOs and that, in contrast to other state-of-the-art simulation techniques, the runtime of quantum algorithms built on MPO decompositions increases only linearly with the size of the register in some cases. The detailed contributions of our study are as follows:

- First, we derive general MPO decompositions of single-qubit and (multi-)controlled quantum gates acting on n -qubit systems without regard to the nearest-neighbor constraint, allowing interactions between arbitrary qubits in the quantum register.
- Second, we consider several examples of fundamental quantum circuits and express them as compact MPOs resulting from the concatenation of multiple quantum gates. The derived networks allow for direct analysis in terms of entanglement structure and their action on quantum states.
- Finally, we demonstrate the capabilities of the proposed method by simulating different quantum algorithms and comparing our results with the results computed by Qiskit.

The paper is structured as follows: In Section 2, we briefly introduce quantum states and quantum gates as well as the MPS format. The representation of quantum gates and circuits as MPOs with the aid of different well-known quantum algorithms is described in Section 3. In Section 4, we provide numerical examples of MPS/MPO-based quantum simulation. We conclude in Section 5 with a summary of the main results and potential impact on further research. Supplementary information and detailed derivations of MPO representations can be found in Appendix A.

2 Preliminaries

We define a tensor to be a multidimensional array with n indices, i.e., $\mathbf{T} \in \mathbb{C}^D$ with $\mathbb{C}^D := \mathbb{C}^{d_1 \times \dots \times d_n}$ is a tensor of order n , where $D = (d_1, \dots, d_n) \in \mathbb{N}^n$ is called mode set. In what follows, we will denote tensors by bold letters and refer to an element of a tensor \mathbf{T} using subscript indices. A standard operation that is frequently required below is the tensor product: Given a tensor \mathbf{T} of order n and a tensor \mathbf{U} of order m , the tensor product $\mathbf{T} \otimes \mathbf{U}$ is defined by

$$(\mathbf{T} \otimes \mathbf{U})_{x_1, \dots, x_n, y_1, \dots, y_m} = \mathbf{T}_{x_1, \dots, x_n} \mathbf{U}_{y_1, \dots, y_m},$$

for any possible combination of mode indices.

2.1 Quantum states

To provide a framework for the description of quantum circuits in MPS/MPO format, let us first recapitulate the basic representation of quantum registers comprising multiple qubits. In what follows, we will consider computational basis states of the form

$$|x\rangle = |x_1 x_2 \dots x_n\rangle = |x_1\rangle \otimes \dots \otimes |x_n\rangle,$$

with $x_i \in \{0, 1\}$, in lexicographical order, i.e.,

$$|0 \dots 00\rangle, |0 \dots 01\rangle, |0 \dots 10\rangle, |0 \dots 11\rangle, \dots, |1 \dots 10\rangle, |1 \dots 11\rangle,$$

where $|0\rangle = [1, 0]^\top$ and $|1\rangle = [0, 1]^\top$. By convention, the basis state index x is the binary number encoded by the bits x_i , with x_1 being the most significant bit. A pure quantum state of n qubits can then be written as

$$|\psi\rangle = \sum_{x_1, \dots, x_n=0}^1 \Psi_{x_1, \dots, x_n} \cdot (|x_1\rangle \otimes \dots \otimes |x_n\rangle), \quad (1)$$

where the tensor $\Psi \in \mathbb{C}^{2 \times n}$ represents the wave function, i.e., it contains the probability amplitudes corresponding to each basis state such that $\sum_{x_1, \dots, x_n=0}^1 |\Psi_{x_1, \dots, x_n}|^2 = 1$. A quantum state is called *separable* if it can be written as a *rank-one* tensor, i.e., as a tensor product of n components:

$$|\psi\rangle = |\psi_1 \psi_2 \dots \psi_n\rangle = |\psi_1\rangle \otimes \dots \otimes |\psi_n\rangle = \begin{bmatrix} \psi_{1,0} \\ \psi_{1,1} \end{bmatrix} \otimes \dots \otimes \begin{bmatrix} \psi_{n,0} \\ \psi_{n,1} \end{bmatrix},$$

where $|\psi_i\rangle = [\psi_{i,0}, \psi_{i,1}]^\top$ is a pure state of the i th subsystem. In this case, the entries of Ψ in (1) are given by

$$\Psi_{x_1, \dots, x_n} = \prod_{i=1}^n \psi_{i, x_i}.$$

However, we are interested in expressing not only separable but also highly *entangled* quantum states with the aid of tensor products. To this end, we employ the MPS format, which will be introduced in Section 2.3, to represent any given quantum state as a tensor network. From the corresponding wave functions, we then want to calculate the probability distribution for measuring each basis state as a tensor network. This will be discussed in Section 2.4.

Example 1: Every tensor product of n qubits is an n -qubit state, e.g.,

$$\frac{1}{\sqrt{2}}(|0\rangle - |1\rangle) \otimes \frac{1}{\sqrt{2}}(|0\rangle + |1\rangle) = \frac{1}{2}(|00\rangle + |01\rangle - |10\rangle - |11\rangle) = \frac{1}{2} \begin{bmatrix} 1 \\ -1 \end{bmatrix} \otimes \begin{bmatrix} 1 \\ 1 \end{bmatrix}.$$

The other direction, however, is not true. That is, not every n -qubit state can be written as a tensor product of n qubits. Such states are called *entangled*. Well-known examples of entangled quantum states are the Bell [46], the Greenberger–Horne–Zeilinger [47], and the W states [48]:

$$\begin{aligned} |\Phi^\pm\rangle &= \frac{1}{\sqrt{2}}(|00\rangle \pm |11\rangle), & |\text{GHZ}\rangle &= \frac{1}{\sqrt{2}}(|0\dots 0\rangle + |1\dots 1\rangle), \\ |\Psi^\pm\rangle &= \frac{1}{\sqrt{2}}(|01\rangle \pm |10\rangle), & |\text{W}\rangle &= \frac{1}{\sqrt{n}}(|10\dots 0\rangle + \dots + |0\dots 01\rangle). \end{aligned}$$

2.2 Quantum gates

We will now give an overview of essential quantum gates that we will use to construct quantum circuits. For a more detailed description and information about other quantum gates, we refer to [49, 50]. Figure 1 shows the considered selection of quantum gates in diagrammatic notation.

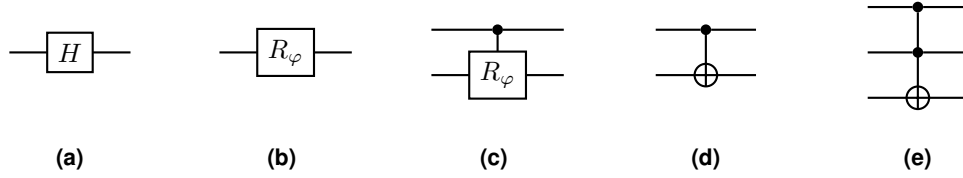


Figure 1: Quantum logic gates: (a) Hadamard gate, (b) phase-shift gate, (c) controlled phase-shift gate, (d) CNOT gate, (e) CCNOT gate. Each line depicts a qubit. We follow the usual convention of a state traversing from left to right. Controlled gates act on two or more qubits, where the control qubits are indicated by a dot.

Two of the most important single-qubit gates in quantum information processing are the *Hadamard gate* and the *phase-shift gate*, given by the matrix representations

$$H = \frac{1}{\sqrt{2}} \begin{bmatrix} 1 & 1 \\ 1 & -1 \end{bmatrix} \quad \text{and} \quad R_\varphi = \begin{bmatrix} 1 & 0 \\ 0 & e^{i\varphi} \end{bmatrix},$$

respectively. See Figure 1 (a) and (b) for the graphical representation of the gates. While the Hadamard gate maps the basis states of a qubit to superpositions of these basis states, a phase-shift gate does not change the probability of measuring $|0\rangle$ or $|1\rangle$ in a fixed basis. Another essential class of operations is given by (multi-)controlled logic gates, i.e., gates acting on two or more qubits where a specific operation is performed on the target qubits only if certain control qubits are in state $|1\rangle$. Examples of controlled gates are the *controlled phase-shift* and the *controlled NOT* gate, see Figure 1 (c) and (d), which can be expressed in canonical format as

$$\text{CPHASE}(\varphi) = \begin{bmatrix} 1 & 0 \\ 0 & 0 \end{bmatrix} \otimes I + C \otimes R_\varphi = I^{\otimes 2} + C \otimes (R_\varphi - I) \cong \begin{bmatrix} 1 & 0 & 0 & 0 \\ 0 & 1 & 0 & 0 \\ 0 & 0 & 1 & 0 \\ 0 & 0 & 0 & e^{i\varphi} \end{bmatrix} \quad (2)$$

and

$$\text{CNOT} = \begin{bmatrix} 1 & 0 \\ 0 & 0 \end{bmatrix} \otimes I + C \otimes \sigma_x = I^{\otimes 2} + C \otimes (\sigma_x - I) \cong \begin{bmatrix} 1 & 0 & 0 & 0 \\ 0 & 1 & 0 & 0 \\ 0 & 0 & 0 & 1 \\ 0 & 0 & 1 & 0 \end{bmatrix}, \quad (3)$$

respectively. Here, C denotes the control matrix and σ_x the Pauli- X gate, given by

$$C = \begin{bmatrix} 0 & 0 \\ 0 & 1 \end{bmatrix} \quad \text{and} \quad \sigma_x = \begin{bmatrix} 0 & 1 \\ 1 & 0 \end{bmatrix}.$$

Note that for the controlled phase-shift gate the positions of the control and phase-shift matrices can be changed, i.e., $\text{CPHASE}(\varphi) = I^{\otimes 2} + (R_\varphi - I) \otimes C$.

An important three-qubit gate with one target and two control qubits is the *Toffoli* or *CCNOT gate*. Only if both control qubits are in state $|1\rangle$ the NOT operation is carried out. Its matrix and canonical representation are given by

$$\text{CCNOT} = I^{\otimes 3} + C \otimes C \otimes (\sigma_x - I) \cong \begin{bmatrix} 1 & 0 & 0 & 0 & 0 & 0 & 0 & 0 \\ 0 & 1 & 0 & 0 & 0 & 0 & 0 & 0 \\ 0 & 0 & 1 & 0 & 0 & 0 & 0 & 0 \\ 0 & 0 & 0 & 1 & 0 & 0 & 0 & 0 \\ 0 & 0 & 0 & 0 & 1 & 0 & 0 & 0 \\ 0 & 0 & 0 & 0 & 0 & 1 & 0 & 0 \\ 0 & 0 & 0 & 0 & 0 & 0 & 0 & 1 \\ 0 & 0 & 0 & 0 & 0 & 0 & 0 & 1 \end{bmatrix}. \quad (4)$$

For the sake of completeness, we address another essential type of two-qubit gate, the so-called *SWAP gate* which exchanges the quantum states of two qubits. Although SWAP gates were exploited in previous studies on MPS/MPO-based representations of quantum states [21, 51] and circuits [41, 42], we will not take SWAP gates explicitly into account. As we will show in Section 3, we can construct compact MPO expressions of gates acting on two or more qubits, even if these are not adjacent.

2.3 Matrix product states and tensor trains

The storage consumption of a tensor $\mathbf{T} \in \mathbb{C}^D$ with $D = (d_1, \dots, d_n) \in \mathbb{N}^n$ can be estimated as $\mathcal{O}(d^n)$, where d is the maximum of all modes. Storing a higher-order tensor is thus in general infeasible for large n since the number of elements of a tensor grows exponentially with the order – this is also known as the *curse of dimensionality*. However, it is possible to mitigate this problem by exploiting low-rank tensor approximations. Our goal is to use the MPS/TT format to efficiently represent quantum states of qubit systems coupled in a one-dimensional chain. A tensor $\mathbf{T} \in \mathbb{C}^D$ is said to be in the MPS format if

$$\mathbf{T} = \sum_{k_0=1}^{r_0} \cdots \sum_{k_d=1}^{r_d} \bigotimes_{i=1}^n \mathbf{T}_{k_{i-1},:,k_i}^{(i)} = \sum_{k_0=1}^{r_0} \cdots \sum_{k_d=1}^{r_d} \mathbf{T}_{k_0,::,k_1}^{(1)} \otimes \cdots \otimes \mathbf{T}_{k_{d-1},::,k_d}^{(d)}.$$

The variables r_i are called *bond dimensions* or *TT ranks* and it holds that $r_0 = r_d = 1$ and $r_i \geq 1$ for $i = 1, \dots, d-1$. The tensors $\mathbf{T}^{(i)} \in \mathbb{C}^{r_{i-1} \times d_i \times r_i}$ are called (*TT*) *cores*. Each element of the tensor \mathbf{T} can be written as

$$\mathbf{T}_{x_1, \dots, x_n} = \mathbf{T}_{1, x_1, :}^{(1)} \mathbf{T}_{:, x_2, :}^{(2)} \cdots \mathbf{T}_{:, x_{n-1}, :}^{(n-1)} \mathbf{T}_{:, x_n, 1}^{(n)}, \quad (5)$$

which explains the origin of the name matrix product states (MPS). Note that here the rank indices start at 1 while the mode indices start at 0. In general, every quantum state can be written as an MPS, but the crucial point is that the ranks determine the storage consumption and expressivity. If the ranks are small enough, we may reduce the storage consumption of an order- n tensor significantly: Instead of an exponential dependence, the storage then depends only linearly on the order and can be estimated as $\mathcal{O}(r^2 dn)$, where r is the maximum over all ranks. That is, if the underlying correlation structure admits such a low-rank decomposition, an enormous reduction in complexity can be achieved. As a result, MPSs are well-suited for describing states with weak entanglement.

A linear operator $\mathbf{G} \in \mathbb{C}^{D \times D}$ in the MPO/TT format, can be written as

$$\mathbf{G} = \sum_{k_0=1}^{R_0} \cdots \sum_{k_d=1}^{R_d} \bigotimes_{i=1}^n \mathbf{G}_{k_{i-1}, :, k_i}^{(i)} = \sum_{k_0=1}^{R_0} \cdots \sum_{k_d=1}^{R_d} \mathbf{G}_{k_0, :, k_1}^{(1)} \otimes \cdots \otimes \mathbf{G}_{k_{d-1}, :, k_d}^{(d)}.$$

Here, the cores are tensors of order 4. Figure 2 (a) and (b) show the graphical representation of an MPS $\mathbf{T} \in \mathbb{C}^D$ and an MPO $\mathbf{G} \in \mathbb{C}^{D \times D}$ with $D = (d_1, \dots, d_5)$, respectively.

In general, for two tensor operators $\mathbf{G}, \mathbf{H} \in \mathbb{C}^{D \times D}$ of order $2n$ with $D = (2, \dots, 2)$, the product $\mathbf{GH} \in \mathbb{C}^{D \times D}$ is defined as

$$(\mathbf{GH})_{x_1, y_1, \dots, x_n, y_n} = \sum_{z_1=0}^1 \cdots \sum_{z_n=0}^1 \mathbf{G}_{x_1, z_1, \dots, x_n, z_n} \mathbf{H}_{z_1, y_1, \dots, z_n, y_n},$$



Figure 2: Graphical representation of the MPS/MPO format: A core is depicted by a circle with different arms indicating the modes of the tensor and the rank indices. (a) Tensor of order 5 as MPS with ranks r_1, r_2, r_3, r_4 . The first and the last core are matrices, the other cores are tensors of order 3. (b) An MPO of order 10 with ranks R_1, R_2, R_3, R_4 . The first and the last core are tensors of order 3, the other cores are tensors of order 4.

with $x_i, y_i \in \{0, 1\}$ for $i = 1, \dots, n$. This means that the product of two MPOs \mathbf{G} and \mathbf{H} is given by

$$\begin{aligned} \mathbf{GH} &= \left(\sum_{k_0=1}^{R_0} \cdots \sum_{k_n=1}^{R_n} \sum_{i=1}^n \bigotimes_{i=1}^n \mathbf{G}_{k_{i-1}, \dots, k_i}^{(i)} \right) \left(\sum_{\ell_0=1}^{R'_0} \cdots \sum_{\ell_n=1}^{R'_n} \sum_{i=1}^n \bigotimes_{i=1}^n \mathbf{H}_{\ell_{i-1}, \dots, \ell_i}^{(i)} \right) \\ &= \sum_{k_0=1}^{R_0} \cdots \sum_{k_n=1}^{R_n} \sum_{\ell_0=1}^{R'_0} \cdots \sum_{\ell_n=1}^{R'_n} \sum_{i=1}^n \bigotimes_{i=1}^n \left(\mathbf{G}_{k_{i-1}, \dots, k_i}^{(i)} \mathbf{H}_{\ell_{i-1}, \dots, \ell_i}^{(i)} \right). \end{aligned} \quad (6)$$

Thus, the ranks of \mathbf{GH} are bounded by the product of the ranks of \mathbf{G} and \mathbf{H} . However, as we will show below, the ranks of resulting circuits can be much smaller in practice. The application of an MPO to an MPS, e.g., a quantum circuit and a quantum state, can be seen as a special case of (6). That is, given an MPO $\mathbf{G} \in \mathbb{C}^{D \times D}$ and an MPS $\mathbf{T} \in \mathbb{C}^D$, the product \mathbf{GT} is given by

$$\begin{aligned} \mathbf{GT} &= \left(\sum_{k_0=1}^{R_0} \cdots \sum_{k_n=1}^{R_n} \sum_{i=1}^n \bigotimes_{i=1}^n \mathbf{G}_{k_{i-1}, \dots, k_i}^{(i)} \right) \left(\sum_{\ell_0=1}^{r_0} \cdots \sum_{\ell_n=1}^{r_n} \sum_{i=1}^n \bigotimes_{i=1}^n \mathbf{T}_{\ell_{i-1}, \dots, \ell_i}^{(i)} \right) \\ &= \sum_{k_0=1}^{R_0} \cdots \sum_{k_n=1}^{R_n} \sum_{\ell_0=1}^{r_0} \cdots \sum_{\ell_n=1}^{r_n} \sum_{i=1}^n \bigotimes_{i=1}^n \left(\mathbf{G}_{k_{i-1}, \dots, k_i}^{(i)} \mathbf{T}_{\ell_{i-1}, \dots, \ell_i}^{(i)} \right). \end{aligned}$$

A convenient way of treating MPS tensors is the core notation, cf. [52–54]. We represent the cores as two-dimensional arrays containing either vectors or matrices as elements. For a given MPS $\mathbf{T} \in \mathbb{C}^D$ with cores $\mathbf{T}^{(i)} \in \mathbb{C}^{r_{i-1} \times d_i \times r_i}$, a single core is written as

$$\llbracket \mathbf{T}^{(i)} \rrbracket = \begin{bmatrix} \mathbf{T}_{1, \dots, 1}^{(i)} & \cdots & \mathbf{T}_{1, \dots, r_i}^{(i)} \\ \vdots & \ddots & \vdots \\ \mathbf{T}_{r_{i-1}, \dots, 1}^{(i)} & \cdots & \mathbf{T}_{r_{i-1}, \dots, r_i}^{(i)} \end{bmatrix}. \quad (7)$$

For a given operator $\mathbf{G} \in \mathbb{C}^{D \times D}$ with cores $\mathbf{G}^{(i)} \in \mathbb{C}^{R_{i-1} \times d_i \times d_i \times R_i}$, each core is written as

$$\llbracket \mathbf{G}^{(i)} \rrbracket = \begin{bmatrix} \mathbf{G}_{1, \dots, 1}^{(i)} & \cdots & \mathbf{G}_{1, \dots, R_i}^{(i)} \\ \vdots & \ddots & \vdots \\ \mathbf{G}_{R_{i-1}, \dots, 1}^{(i)} & \cdots & \mathbf{G}_{R_{i-1}, \dots, R_i}^{(i)} \end{bmatrix}. \quad (8)$$

We then use the notation

$$\mathbf{T} = \llbracket \mathbf{T}^{(1)} \rrbracket \otimes \cdots \otimes \llbracket \mathbf{T}^{(n)} \rrbracket \quad \text{and} \quad \mathbf{G} = \llbracket \mathbf{G}^{(1)} \rrbracket \otimes \cdots \otimes \llbracket \mathbf{G}^{(n)} \rrbracket.$$

The corresponding operations can be regarded as a generalization of the standard matrix multiplication, where the cores contain matrices as elements instead of scalars. Here, we first compute the tensor products of the corresponding elements and then sum over the corresponding columns and rows. The advantage of the core notation is not only that we can derive compact representations of quantum states and logic gates, but that we can also easily manipulate the cores by linear transformations, which is described in Appendix A.1.1.

Example 2: Let us consider the W state introduced in Example 1. The rank of its canonical representation is n which means that n rank-one tensors (comprising n vectors) are needed to express the amplitude tensor as a sum of tensor products, leading to a storage consumption of $O(2n^2)$ (without exploiting sparsity). However, the MPS format allows us to represent the wave function of $|W\rangle$ in a more compact form as

$$\Psi = \frac{1}{\sqrt{n}} \llbracket |1\rangle \quad |0\rangle \rrbracket \otimes \llbracket \begin{bmatrix} |0\rangle \\ |1\rangle \end{bmatrix} \quad |0\rangle \rrbracket \otimes \cdots \otimes \llbracket \begin{bmatrix} |0\rangle \\ |1\rangle \end{bmatrix} \quad |0\rangle \rrbracket \otimes \llbracket \begin{bmatrix} |0\rangle \\ |1\rangle \end{bmatrix} \rrbracket, \quad (9)$$

which has a rank of 2, leading to storage consumption of $O(r^2 dn) = O(8n)$. For the sake of clarity, we omit core elements that are equal to the vector of all zeros. The decomposition in (9) shows, on the one hand, that MPS representations may require less memory and, on the other hand, that the core notation allows for a more compact representation of qubit states. The form of the decomposition in (9) is a special case of so-called SLIM decompositions used for expressing nearest-neighbor interaction systems in TT format, see [54]. As an example of the core manipulation of MPS/MPO decompositions (see Appendix A.1.1), consider the CNOT gate. From (3), we deduce its representation in core notation as

$$\text{CNOT} = \llbracket I \quad C \rrbracket \otimes \llbracket \begin{bmatrix} I \\ \sigma_x - I \end{bmatrix} \rrbracket.$$

An alternative MPS representation can be derived as follows:

$$\begin{aligned} \text{CNOT} &= \llbracket I \quad C \rrbracket \otimes \left(\begin{bmatrix} 1 & 0 \\ -1 & 1 \end{bmatrix} \cdot \llbracket \begin{bmatrix} I \\ \sigma_x \end{bmatrix} \rrbracket \right) \\ &= \left(\llbracket I \quad C \rrbracket \cdot \begin{bmatrix} 1 & 0 \\ -1 & 1 \end{bmatrix} \right) \otimes \llbracket \begin{bmatrix} I \\ \sigma_x \end{bmatrix} \rrbracket \\ &= \llbracket I - C \quad C \rrbracket \otimes \llbracket \begin{bmatrix} I \\ \sigma_x \end{bmatrix} \rrbracket. \end{aligned}$$

2.4 Probability distributions and generative sampling

Suppose the wave function is given in form of an MPS $\Psi \in \mathbb{C}^{2^{\otimes n}}$. As explained in [44, 45], it is possible to directly sample from the probability distribution given by the tensor \mathbf{P} with

$$\mathbf{P}_{x_1, \dots, x_n} := \mathbb{P}(x) = |\Psi_{x_1, \dots, x_n}|^2 / Z,$$

where $Z = \sum_{x_1, \dots, x_n} |\Psi_{x_1, \dots, x_n}|^2$ is the normalization factor. In what follows, we assume that Ψ is already normalized, thus $Z = 1$. The idea is to exploit the orthonormality of the TT cores to generate samples qubit-wise by constructing conditional probability distributions from segments of the tensor \mathbf{P} . The tensor \mathbf{P} can be written as

$$\mathbf{P}_{x_1, \dots, x_n} = \overline{\Psi_{x_1, \dots, x_n}} \Psi_{x_1, \dots, x_n} \iff \mathbf{P} = \text{diag}(\overline{\Psi}) \Psi,$$

see Figure 3 (a). Here, $\text{diag}(\cdot)$ denotes a diagonal MPO, see Appendix A.1.3.

Provided that the number of qubits is small enough so that it can be stored in the full format, one can directly construct the marginal probability tensor corresponding to the measured qubits. That is, by summing the joint probability distribution over all values of the unmeasured qubits, i.e., multiplying the corresponding modes with the vector $\mathbf{1} = [1, 1]^T$, and contracting all cores, we obtain a tensor

$$\mathbf{P}_{x_1, \dots, x_m}^I = \sum_{x_j, j \notin I} \mathbf{P}_{x_1, \dots, x_n}$$

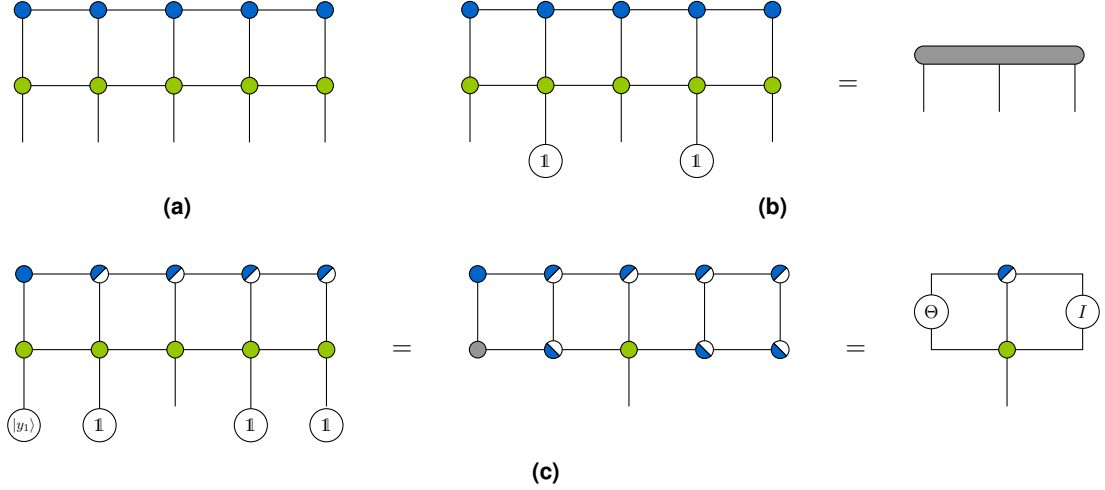


Figure 3: Probability distributions and generative sampling: (a) Probability tensor \mathbf{P} . Green circles represent the cores of $\text{diag}(\bar{\Psi})$ and blue circles the cores of Ψ . (b) Direct computation of the marginal probability tensor \mathbf{P}^I in full format. (c) Construction of conditional probability vector P^i for generative sampling. Here, all cores of Ψ except the first are right-orthonormalized (half-filled circles) before constructing the network. The cores are orthonormal with respect to the modes at the blank halves of the half-filled circles.

where $I = \{i_1, \dots, i_m\} \subseteq \{1, \dots, n\}$, with $m \leq n$, denotes the index set of the qubits to be measured. See Figure 3 (b) for a graphical representation of \mathbf{P}^I . If the number of qubits is large, it is impossible to compute the (marginal) probability tensor in the full format. Additionally, we are here rather interested in a generative sampling strategy of the outputs of a given quantum circuit. Given the tensor Ψ as MPS, we first right-orthonormalize the last $n - 1$ cores, e.g., by applying a sequence of singular value decompositions (SVDs), cf. Appendix A.1.2. The sampling procedure depicted in Figure 3 (c) then works as follows: Suppose we want to measure the i th qubit of our register. To do so, we sum over all modes with index $j > i$. Modes with index $j < i$ are either contracted with a unit basis vector $|y_j\rangle$ (i.e., y_j was measured before at position j) or also multiplied by $\mathbb{1}$ (i.e., the j th qubit is not measured and, thus, not considered for sampling). Note that summation of a mode in this case results in the conjugate transpose of the corresponding right-orthonormal core of Ψ . Therefore, the segment of the tensor network to the right of the i th core of \mathbf{P} is equal to an identity matrix. The left part can be contracted iteratively so that we obtain a matrix Θ at each step of the sampling. Given an index set I as above, the resulting vector at position $i_k \in I$, $1 \leq k \leq m$, is then given by

$$P^{i_k} = \sum_{x_{i_{k+1}}, \dots, x_{i_m}} \mathbf{P}^I_{y_{i_1}, \dots, y_{i_{k-1}}, \dots, x_{i_{k+1}}, \dots, x_{i_m}}$$

and contains the conditional probabilities for measuring x_i as the i th qubit, given that the states $y_{i_1}, \dots, y_{i_{k-1}}$ are measured on the qubits i_1, \dots, i_{k-1} . By successively drawing the bit values from the conditional probabilities in P^i , $i \in I$, we generate a sample according to the probability distribution given by \mathbf{P} .

Remark 1: The process of postselection, i.e., conditioning on the outcome of a measurement on certain qubits, means to condition the probability distribution given by \mathbf{P} . That is, after postselecting, e.g., q_1, \dots, q_p , we consider the probabilities

$$\mathbb{P}(x_{p+1} = y_{p+1}, \dots, x_n = y_n \mid x_1 = y_1, \dots, x_p = y_p) = \frac{\mathbf{P}_{y_1, \dots, y_n}}{\mathbf{P}^I_{y_1, \dots, y_p}},$$

where $I = \{1, \dots, p\}$. The outcomes when measuring q_{p+1}, \dots, q_n then strictly obey the marginal

probability distribution given by \mathbf{P}^J with $J = \{p+1, \dots, n\}$ since

$$\sum_{\substack{x_1, \dots, x_p \\ \mathbf{P}_{x_1, \dots, x_p}^I > 0}} \mathbf{P}_{x_1, \dots, x_p}^I \frac{\mathbf{P}_{x_1, \dots, x_n}}{\mathbf{P}_{x_1, \dots, x_p}^I} = \sum_{\substack{x_1, \dots, x_p \\ \mathbf{P}_{x_1, \dots, x_p}^I > 0}} \mathbf{P}_{x_1, \dots, x_n} = \sum_{x_1, \dots, x_p} \mathbf{P}_{x_1, \dots, x_n} = \mathbf{P}_{x_{p+1}, \dots, x_n}^J.$$

Given a right-orthonormalized MPS Ψ , the computational complexity of the sampling procedure is mainly determined by the contractions of the tensor cores. If we store the matrix Θ , see Figure 3 (c), and adapt it successively after each sampling step, the overall cost is $O(snr^3)$, where s denotes the number of samples and r the maximum rank of Ψ .

3 Representation of quantum gates and circuits as MPOs

We will now explain how to derive explicit MPO representations of quantum circuits. In particular, we will use the core notation of the TT format, see Section 2.3, which allows us to derive compact expressions of (interconnected) quantum gates. Considering a single-qubit gate A , e.g., a Hadamard gate, acting on an n -qubit system, the tensor operator \mathbf{G} corresponding to the application of A to the qubit at position p is given by

$$\mathbf{G} = I^{\otimes(p-1)} \otimes A \otimes I^{\otimes(n-p)} = I \otimes \dots \otimes I \otimes \underbrace{A}_{\text{position } p} \otimes I \otimes \dots \otimes I.$$

Any controlled gate acting on a quantum register with n qubits has a rank-2 representation of the form

$$\begin{aligned} \mathbf{G} &= I^{\otimes n} + I^{\otimes(p-1)} \otimes C \otimes I^{\otimes(q-p-1)} \otimes (A - I) \otimes I^{\otimes(n-q)} \\ &= \underbrace{[I] \otimes \dots \otimes [I]}_{\text{position } p} \otimes \underbrace{\begin{bmatrix} I & C \end{bmatrix}}_{\text{position } p} \otimes \dots \otimes \underbrace{\begin{bmatrix} I & I \end{bmatrix}}_{\text{position } q} \otimes \underbrace{\begin{bmatrix} I & A-I \end{bmatrix}}_{\text{position } q} \otimes [I] \otimes \dots \otimes [I], \end{aligned}$$

where p is the position of the control qubit and q the position of the target qubit. Again, we here use blanks for core elements equal to the matrix of all zeros. If $p > q$, the corresponding matrices C and $A - I$ are interchanged. If we apply a three-qubit gate, e.g., a CCNOT gate (4), to an n -qubit system, we obtain the augmented decomposition

$$\begin{aligned} \mathbf{G} &= [I] \otimes \dots \otimes [I] \otimes \underbrace{\begin{bmatrix} I & C \end{bmatrix}}_{\text{position } p_1} \otimes \begin{bmatrix} I & I \end{bmatrix} \otimes \dots \otimes \begin{bmatrix} I & I \end{bmatrix} \otimes \underbrace{\begin{bmatrix} I & C \end{bmatrix}}_{\text{position } p_2} \otimes \dots \\ &\quad \otimes \begin{bmatrix} I & I \end{bmatrix} \otimes \dots \otimes \begin{bmatrix} I & I \end{bmatrix} \otimes \underbrace{\begin{bmatrix} I & A-I \end{bmatrix}}_{\text{position } q} \otimes [I] \otimes \dots \otimes [I], \end{aligned}$$

where p_1 and p_2 are the positions of the control qubits and q the position of the target qubit. Note that any (multi-)control quantum gate can be represented by a tensor with canonical and MPS ranks bounded by 2.

In Sections 3.1–3.3, we will consider specific examples of well-known quantum circuits and express them as compact MPOs resulting from the multiplication/concatenation of several quantum gates. Numerical experiments pertaining to the application of these circuits to quantum states in MPS/TT format can be found in Section 4.

3.1 Quantum full adder

The *quantum full adder* (QFA) is the quantum analogue of a full-adder circuit used in classical computers to add up to three bits. Due to reversibility requirements, the QFA acts on four qubits: The input qubits are $|C_{\text{in}}\rangle$, $|A\rangle$, $|B\rangle$, and $|0\rangle$ and the output qubits are $|S\rangle$, $|A\rangle$, $|B\rangle$, and $|C_{\text{in}}\rangle$. Figure 4 shows the QFA implementation proposed in [55].

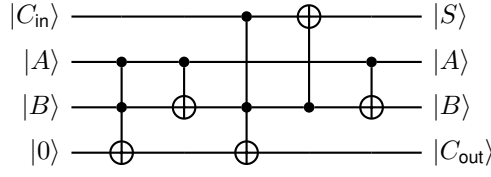


Figure 4: Quantum full adder: Here, the QFA consists of three CNOT and two CCNOT gates.

The qubit $|C_{\text{in}}\rangle$ is carried in from the previous (less-significant) stage of a multi-digit addition. The circuit produces the sum of the input qubits including a carry-out signal for the overflow into the next digit. The corresponding operator is given by the concatenation

$$\mathbf{G} = \text{CNOT}(2 | 3) \cdot \text{CNOT}(3 | 1) \cdot \text{CCNOT}(1, 3 | 4) \cdot \text{CNOT}(2 | 3) \cdot \text{CCNOT}(2, 3 | 4),$$

where $\text{CNOT}(p | q)$ and $\text{CCNOT}(p_1, p_2 | q)$ denote the (controlled-)controlled NOT gates with control qubits p, p_1, p_2 and target qubit q . That is, using the MPO representation of the involved gates, we consider the product

$$\begin{aligned} \mathbf{G} = & \quad I \quad \otimes \begin{bmatrix} I & C \end{bmatrix} \otimes \begin{bmatrix} I \\ \sigma_x - I \end{bmatrix} \otimes I \\ & \cdot \begin{bmatrix} I & \sigma_x - I \end{bmatrix} \otimes \begin{bmatrix} I \\ I \end{bmatrix} \otimes \begin{bmatrix} I \\ C \end{bmatrix} \otimes I \\ & \cdot \begin{bmatrix} I & C \end{bmatrix} \otimes \begin{bmatrix} I \\ I \end{bmatrix} \otimes \begin{bmatrix} I \\ C \end{bmatrix} \otimes \begin{bmatrix} I \\ \sigma_x - I \end{bmatrix} \\ & \cdot \quad I \quad \otimes \begin{bmatrix} I & C \end{bmatrix} \otimes \begin{bmatrix} I \\ \sigma_x - I \end{bmatrix} \otimes I \\ & \cdot \quad I \quad \otimes \begin{bmatrix} I & C \end{bmatrix} \otimes \begin{bmatrix} I \\ C \end{bmatrix} \otimes \begin{bmatrix} I \\ \sigma_x - I \end{bmatrix}. \end{aligned} \quad (10)$$

Although the theoretical rank bounds of an MPO decomposition of an operator in $\mathbb{C}^{(2 \times 2)^{\times 4}}$ are given by $(1, 4, 16, 4, 1)$, we are able to provide an exact representation with much smaller ranks. In fact, the operator \mathbf{G} can be written as

$$\mathbf{G} = \begin{bmatrix} \sigma_x C_0 & I & \sigma_x C_1 \end{bmatrix} \otimes \begin{bmatrix} C_0 & C_1 \\ C_0 & C_1 \end{bmatrix} \otimes \begin{bmatrix} C_1 \\ C_0 \\ C_1 \\ C_0 \end{bmatrix} \otimes \begin{bmatrix} I \\ \sigma_x \end{bmatrix}, \quad (11)$$

with control matrices $C_0 = I - C$ and $C_1 = C$. A proof of correctness of (11) can be found in Appendix A.2.1. The coupling between the different dimensions directly reflects the action of the QFA on different basis states. For instance, if both qubits $|A\rangle$ and $|B\rangle$ are in state $|0\rangle$, we have

$$\begin{aligned} |S, A, B, C_{\text{out}}\rangle &= \mathbf{G} |C_{\text{in}}, A, B, 0\rangle \\ &= \begin{bmatrix} \sigma_x C_0 |C_{\text{in}}\rangle & |C_{\text{in}}\rangle & \sigma_x C_1 |C_{\text{in}}\rangle \end{bmatrix} \otimes \begin{bmatrix} |0\rangle & 0 & 0 & 0 \\ 0 & |0\rangle & 0 & 0 \\ 0 & 0 & |0\rangle & 0 \end{bmatrix} \otimes \begin{bmatrix} 0 & 0 \\ |0\rangle & 0 \\ 0 & 0 \\ 0 & |0\rangle \end{bmatrix} \otimes \begin{bmatrix} |0\rangle \\ |1\rangle \end{bmatrix} \\ &= \begin{bmatrix} \sigma_x C_0 |C_{\text{in}}\rangle & |C_{\text{in}}\rangle & \sigma_x C_1 |C_{\text{in}}\rangle \end{bmatrix} \otimes \begin{bmatrix} 0 & 0 \\ |0, 0\rangle & 0 \\ 0 & 0 \end{bmatrix} \otimes \begin{bmatrix} |0\rangle \\ |1\rangle \end{bmatrix} \\ &= |C_{\text{in}}, 0, 0, 0\rangle. \end{aligned}$$

Analogously, we get $|S, A, B, C_{\text{out}}\rangle = |C_{\text{in}}, 1, 1, 1\rangle$ when $|A\rangle = |B\rangle = |1\rangle$. In Section Section 4.1, we will use the carry-in and carry-out qubits to couple several QFAs.

3.2 Simon's algorithm

We begin our considerations with the first quantum algorithm that demonstrated an exponential speed-up compared to the best classical algorithm, namely *Simon's algorithm* [5, 56]. Let $f: \{0, 1\}^n \rightarrow \{0, 1\}^n$ be a function that is either *one-to-one* (maps exactly one input to every unique output) or *two-to-one* (maps exactly two inputs to every unique output) such that

$$f(x) = f(y) \iff x = y \oplus b$$

for all $x, y \in \{0, 1\}^n$, where \oplus denotes bitwise XOR. The vector $b \in \{0, 1\}^n$ is called a *hidden bitstring* and the aim is to determine b (also called *Simon's problem*) minimizing the number of evaluations of f . Even though Simon's algorithm assumes the existence of a potentially highly complex black-box oracle U_f for the function evaluation of f , see below, it was an important step in quantum computing as it solves Simon's problem exponentially faster and with exponentially fewer queries than the best classical algorithm and served as an inspiration for Shor's algorithm, see Section 4.3. It was shown recently that Simon's algorithm can also be used to attack certain types of cryptosystems [57, 58]. The method involves the following steps:

- 1) Initialize two n -qubit registers with the zero state, the first one as input and the second one as output of the oracle.
- 2) Apply Hadamard gates to the first register to create a superposition of all possible inputs.
- 3) Apply the oracle function so that $|x, 0^n\rangle \mapsto |x, f(x)\rangle$.
- 4) Measure the second register, $f(x)$, thus collapse a superposition over the first register, i.e., $\frac{1}{\sqrt{2}}(|x\rangle + |x \oplus b\rangle)$.
- 5) Apply Hadamard gates to the first register.
- 6) Measure the first register and obtain a bitstring z with bitwise inner product $z \cdot b = 0 \pmod{2}$.

The corresponding quantum circuit is shown in Figure 5 (a). The postprocessing step, i.e., determining the hidden bitstring b from measurements z_1, \dots, z_m , can then be realized on a classical computer by solving a system of linear equations with mod-2 arithmetic, where a solution $b = 00 \dots 0$ represents the case of a one-to-one function f .

First, we reorder the qubits in both registers, see Figure 5 (b), so that a low-rank decomposition of the circuit can be constructed. Let us consider the oracle U'_f shown in Figure 5 (c) acting on $2 \cdot 4 = 8$ qubits. By construction, the associated gate groups \mathbf{G}_2 and \mathbf{G}_3 encode the hidden bitstring $b = 1010$ where \mathbf{G}_2 copies the content of the first register to the second register and \mathbf{G}_3 flips the first and third qubit of the second register if the leading qubit of the first register is in state 1. This becomes clear by considering the following mappings which show that the oracle indeed satisfies $f(x) = f(x \oplus b)$:

$$0i_20i_4 \mapsto 0i_20i_4, \quad 0i_21i_4 \mapsto 0i_21i_4, \quad 1i_20i_4 \mapsto 0i_21i_4, \quad 1i_21i_4 \mapsto 0i_20i_4. \quad (12)$$

Defining $C_0 = I - C$ and $C_1 = C$ again, it follows that \mathbf{G}_2 can be represented as

$$\begin{aligned} \mathbf{G}_2 &= (C_0 \otimes I + C_1 \otimes \sigma_x) \otimes (C_0 \otimes I + C_1 \otimes \sigma_x) \otimes (C_0 \otimes I + C_1 \otimes \sigma_x) \otimes (C_0 \otimes I + C_1 \otimes \sigma_x) \\ &= \begin{bmatrix} C_0 & C_1 \end{bmatrix} \otimes \begin{bmatrix} I \\ \sigma_x \end{bmatrix} \otimes \begin{bmatrix} C_0 & C_1 \end{bmatrix} \otimes \begin{bmatrix} I \\ \sigma_x \end{bmatrix} \otimes \begin{bmatrix} C_0 & C_1 \end{bmatrix} \otimes \begin{bmatrix} I \\ \sigma_x \end{bmatrix} \otimes \begin{bmatrix} C_0 & C_1 \end{bmatrix} \otimes \begin{bmatrix} I \\ \sigma_x \end{bmatrix}, \end{aligned}$$

and the whole circuit $\mathbf{G} = \mathbf{G}_4 \cdot \mathbf{G}_3 \cdot \mathbf{G}_2 \cdot \mathbf{G}_1$ has an MPO representation in the form of

$$\begin{aligned} \mathbf{G} &= \begin{bmatrix} A & B \end{bmatrix} \otimes \begin{bmatrix} I \\ I \end{bmatrix} \otimes \begin{bmatrix} A & B & A & B \end{bmatrix} \otimes \begin{bmatrix} I \\ \sigma_x \\ I \\ \sigma_x \end{bmatrix} \\ &\otimes \begin{bmatrix} A & B \\ B & A \end{bmatrix} \otimes \begin{bmatrix} I \\ \sigma_x \end{bmatrix} \otimes \begin{bmatrix} A & B \end{bmatrix} \otimes \begin{bmatrix} I \\ \sigma_x \end{bmatrix}, \end{aligned} \quad (13)$$

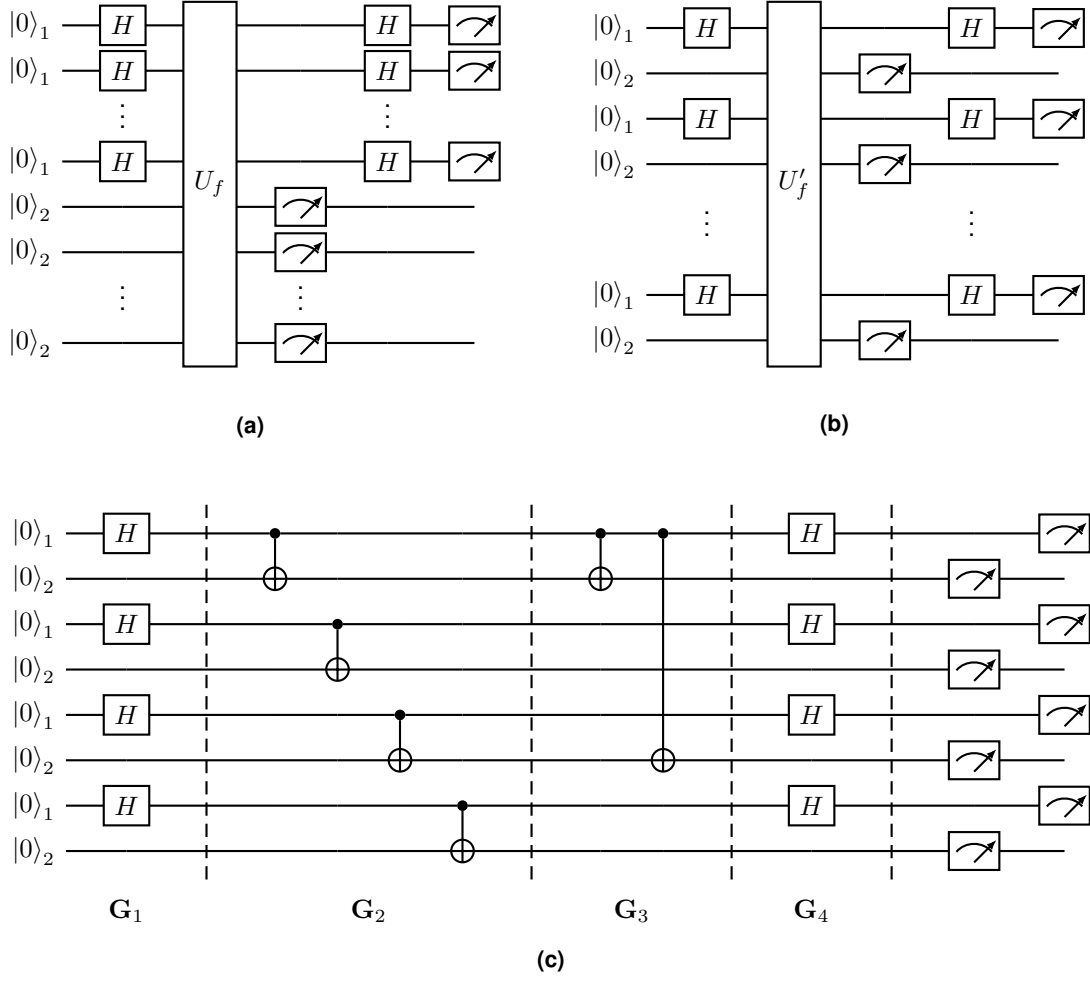


Figure 5: Simon's circuit: (a) Diagrammatic notation of Simon's algorithm. The qubits $|0\rangle_1$ and $|0\rangle_2$ belong to the first and second register, respectively. (b) Reordering of the quantum registers so that the qubits alternate between the first and the second register. (c) Example of Simon's algorithm involving an oracle based on CNOT gates. Since the Hadamard gates on the first register and the measurements on the last register act on disjoint sets of qubits and thus commute, we can change the order of these operations.

where $A = HC_0H = \frac{1}{2} \begin{bmatrix} 1 & 1 \\ 1 & 1 \end{bmatrix}$ and $B = HC_1H = \frac{1}{2} \begin{bmatrix} 1 & -1 \\ -1 & 1 \end{bmatrix}$. See Appendix A.2.2 for a detailed derivation of the above expressions. Note that due to the reordering of the qubits we can write \mathbf{G} as an MPO with ranks bounded by 4. Furthermore, the NOT operation on the second qubit vanishes since the CNOT gates in G_2 and G_3 acting on the first two qubits cancel each other out. The application of the operator given in (13) to the zero state yields the quantum state

$$\begin{aligned}
 \mathbf{G} |0^{2n}\rangle &= \mathbf{G} \cdot \left(\begin{bmatrix} 1 \\ 0 \end{bmatrix} \otimes \begin{bmatrix} 1 \\ 0 \end{bmatrix} \otimes \cdots \otimes \begin{bmatrix} 1 \\ 0 \end{bmatrix} \right) \\
 &= \frac{1}{4} \cdot \begin{bmatrix} |+\rangle & |-\rangle \end{bmatrix} \otimes \begin{bmatrix} |0\rangle \\ |0\rangle \end{bmatrix} \otimes \begin{bmatrix} |+\rangle & |-\rangle \\ |+\rangle & |-\rangle \end{bmatrix} \otimes \begin{bmatrix} |0\rangle \\ |1\rangle \end{bmatrix} \\
 &\quad \otimes \begin{bmatrix} |+\rangle & |-\rangle \\ |-\rangle & |+\rangle \end{bmatrix} \otimes \begin{bmatrix} |0\rangle \\ |1\rangle \end{bmatrix} \otimes \begin{bmatrix} |+\rangle & |-\rangle \end{bmatrix} \otimes \begin{bmatrix} |0\rangle \\ |1\rangle \end{bmatrix}.
 \end{aligned}$$

where $|+\rangle$ and $|-\rangle$ denote the X-basis states $\frac{1}{\sqrt{2}}[1, 1]^\top$ and $\frac{1}{\sqrt{2}}[1, -1]^\top$, respectively. As we can directly see, the wave function is always zero if we consider the first bit of the second register (corresponds to the second TT core) to be in state $|1\rangle$. This coincides with the possible mappings given in (12). We construct the probability tensor $\mathbf{P} \in \mathbb{R}^{2 \times 8}$ as described in Section 2.4. As shown above, the postselection on a measurement outcome in the second register, say $j_1 j_2 j_3 j_4$, corresponds to computing the conditional probability tensor $\mathbf{P}^C = \mathbf{P}_{:,j_1, :, j_2, :, j_3, :, j_4} \in \mathbb{R}^{2 \times 4}$. That is, the probability of obtaining the bitstring $i_1 i_2 i_3 i_4$ when we measure the first register (after obtaining $j_1 j_2 j_3 j_4$ on the second register) is given by $\mathbf{P}_{i_1, i_2, i_3, i_4}^C = \mathbf{P}_{i_1, j_1, i_2, j_2, i_3, j_3, i_4, j_4}$. Finally, the probability distribution of all possible outcomes of the first register is given by the marginal probability tensor

$$\mathbf{P}^M = \sum_{j_1, j_2, j_3, j_4=1}^2 \mathbf{P}_{:,j_1, :, j_2, :, j_3, :, j_4} = \frac{1}{8} \cdot \begin{bmatrix} |0\rangle & |1\rangle \end{bmatrix} \otimes \begin{bmatrix} |+\rangle & |-\rangle \end{bmatrix} \otimes \begin{bmatrix} |0\rangle \\ |1\rangle \end{bmatrix} \otimes \begin{bmatrix} |+\rangle \end{bmatrix}.$$

The set of bitstrings with non-zero probability is given by

$$L = \{0000, 0001, 0100, 0101, 1010, 1011, 1110, 1111\},$$

each bitstring having a probability of 12.5%, and it turns out that 1010 is the only bitstring $b \neq 0$ satisfying $z \cdot b = 0 \pmod{2}$ for each $z \in L$.

3.3 (Inverse) Quantum Fourier transform

The quantum counterpart of the classical discrete Fourier transform is the *quantum Fourier transform* (QFT) [59], which performs the transformation on the amplitude tensor of a quantum state. Even compared to the most efficient implementations on classical computers like fast Fourier transform, QFT provides an exponential speed-up on quantum computers. Due to the fact that the result of the QFT is not directly accessible as a whole, the application areas of the classical and the quantum versions of the Fourier transform differ. However, QFT is an essential part of various quantum algorithms, in particular Shor's algorithm for finding the prime factors of a given integer [3]. It maps a state in the computational basis to a state in the Fourier basis. That is, given a basis state $|x\rangle = |x_1 \dots x_n\rangle = |x_1\rangle \otimes \dots \otimes |x_n\rangle$ with $x_j \in \{0, 1\}$ for $j = 1, \dots, n$, the result after applying the QFT is

$$\text{QFT } |x\rangle = \frac{1}{\sqrt{N}} \sum_{y=0}^{N-1} e^{\frac{2\pi i}{N} xy} |y\rangle = \frac{1}{\sqrt{N}} (|0\rangle + e^{2\pi i 0 \cdot x_n} |1\rangle) \otimes \dots \otimes (|0\rangle + e^{2\pi i 0 \cdot x_1 \dots x_n} |1\rangle), \quad (14)$$

where $N = 2^n$ and $0.x_n, \dots, 0.x_1 \dots x_n$ denote fractional binary numbers, i.e., $0.y_1 \dots y_m = \sum_{j=1}^m y_j 2^{-j}$. Figure 6 (a) shows the corresponding circuit diagram. The quantum circuit can be divided into n gate groups \mathbf{G}_i , each composed of Hadamard and controlled phase gates acting on qubit i . The single-qubit gates R_k are defined as the diagonal matrices $\text{diag}\left(1, e^{\frac{2\pi i}{2^k}}\right)$.

Note that the outputs $\psi_i = \frac{1}{\sqrt{2}}(|0\rangle + e^{2\pi i 0 \cdot x_i \dots x_n} |1\rangle)$ are in reverse order. However, we omit a reordering (by using SWAP gates) because we can simply read the resulting MPS backwards. While \mathbf{G}_n is given by $\mathbf{G}_n = I^{\otimes(n-1)} \otimes H$, each gate group \mathbf{G}_i of the QFT with $1 \leq i \leq n-1$ can be represented as

$$\mathbf{G}_i = \frac{1}{\sqrt{2}} I^{\otimes(i-1)} \otimes \begin{bmatrix} 1 & 1 \\ 0 & 0 \end{bmatrix} \begin{bmatrix} 0 & 0 \\ 1 & -1 \end{bmatrix} \otimes \begin{bmatrix} I & \\ & R_2 \end{bmatrix} \otimes \dots \otimes \begin{bmatrix} I & \\ & R_{n-i} \end{bmatrix} \otimes \begin{bmatrix} I \\ R_{n-i+1} \end{bmatrix}. \quad (15)$$

The derivation of the above decomposition is shown in Appendix A.2.3. An analog canonical expression in terms of Kronecker products can be found in [60]. From (14) we know that $\text{QFT } |x\rangle$ can be written as a rank-one tensor for any basis state $|x\rangle$. Even though the operator in (15) has rank 2, we can easily show a form of rank preservation which induces the rank-one decomposition of $\text{QFT } |x\rangle$. Given a quantum state

$$|\psi\rangle = |\psi_1\rangle \otimes \dots \otimes |\psi_{i-1}\rangle \otimes |x_i\rangle \otimes \dots \otimes |x_n\rangle,$$

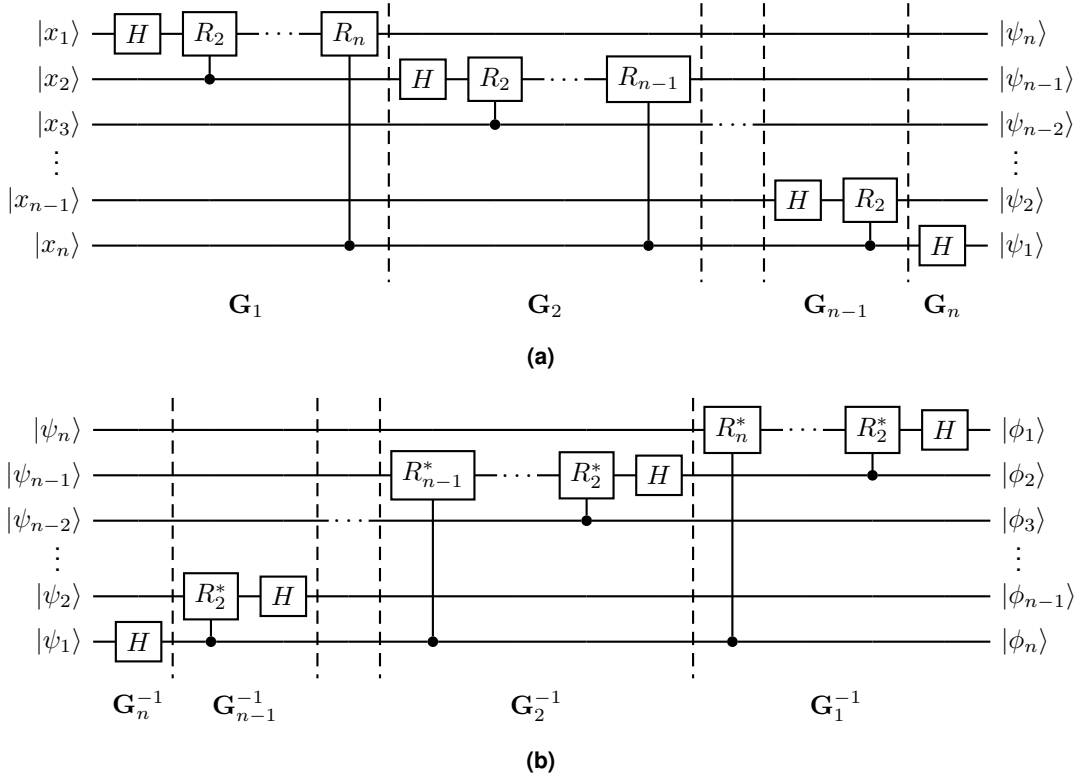


Figure 6: (Inverse) quantum Fourier transform: (a) QFT applied to a basis state $|x\rangle$ results in a quantum state $|\psi\rangle$. To reverse the ordering of the qubits at most $n/2$ would have to be included at the end of the circuit. (b) The application of the inverse QFT to a (reordered) Fourier state yields a quantum state $|\phi\rangle$ in computational basis.

where $\psi_1, \dots, \psi_{i-1}$ are arbitrary superpositions and x_i, \dots, x_n are basis states, we have

$$\begin{aligned}
\mathbf{G}_i |\psi\rangle &= \frac{1}{\sqrt{2}} |\psi_1 \dots \psi_{i-1}\rangle \otimes \left[|0\rangle e^{2\pi i 0.x_i 00\dots 000} |1\rangle \right] \otimes \left[|x_{i+1}\rangle e^{2\pi i 0.x_{i+1} 0\dots 000} |x_{i+1}\rangle \right] \otimes \dots \\
&\quad \dots \otimes \left[|x_{n-1}\rangle e^{2\pi i 0.000\dots 0x_{n-1} 0} |x_{n-1}\rangle \right] \otimes \left[|x_n\rangle e^{2\pi i 0.000\dots 00x_n} |x_n\rangle \right] \\
&= \frac{1}{\sqrt{2}} |\psi_1 \dots \psi_{i-1}\rangle \otimes \left[|0\rangle e^{2\pi i 0.x_i 00\dots 000} |1\rangle \right] \otimes \left[e^{2\pi i 0.x_{i+1} \dots x_n} |x_{i+1} \dots x_n\rangle \right] \\
&= \frac{1}{\sqrt{2}} |\psi_1 \dots \psi_{i-1}\rangle \otimes (|0\rangle + e^{2\pi i 0.x_i \dots x_n} |1\rangle) \otimes |x_{i+1} \dots x_n\rangle.
\end{aligned}$$

Thus, it holds that

$$\mathbf{G}_i \cdot \dots \cdot \mathbf{G}_1 |x\rangle = \frac{1}{\sqrt{2^i}} (|0\rangle + e^{2\pi i 0.x_1 \dots x_n} |1\rangle) \otimes \dots \otimes (|0\rangle + e^{2\pi i 0.x_i \dots x_n} |1\rangle) \otimes |x_{i+1} \dots x_n\rangle,$$

which corresponds to the definition of the QFT with reversed order of the qubits.

The *inverse QFT* is depicted in Figure 6 (b). The different gate groups are the inverse operators of $\mathbf{G}_1, \dots, \mathbf{G}_n$ as given above. Therefore, each gate group \mathbf{G}_i^{-1} of the inverse QFT consists of the adjoints, i.e., the conjugate transposes, of the controlled phase-shift gates in \mathbf{G}_i and a Hadamard gate. Using the core notation, we can express \mathbf{G}_i^{-1} as

$$\mathbf{G}_i^{-1} = \frac{1}{\sqrt{2}} I^{\otimes(i-1)} \otimes \left[\begin{bmatrix} 1 & 0 \\ 1 & 0 \end{bmatrix} \begin{bmatrix} 0 & 1 \\ 0 & -1 \end{bmatrix} \right] \otimes \left[I \quad R_2^* \right] \otimes \dots \otimes \left[I \quad R_{n-i}^* \right] \otimes \left[\begin{matrix} I \\ R_{n-i+1}^* \end{matrix} \right].$$

Analogously to the QFT, we can show that $\mathbf{G}_i^{-1} |\psi\rangle$ has a rank-one representation if ψ_j is either 0 or 1

for $j = 1, \dots, n$. We then have

$$\text{QFT}^{-1} |\psi\rangle = \frac{1}{\sqrt{N}} \sum_{y=0}^{N-1} e^{-\frac{2\pi i}{N} \psi y} |y\rangle = \frac{1}{\sqrt{N}} (|0\rangle + e^{-2\pi i 0 \cdot \psi_n} |1\rangle) \otimes \dots \otimes (|0\rangle + e^{-2\pi i 0 \cdot \psi_1 \dots \psi_n} |1\rangle).$$

In Section 4.3, we will employ the inverse QFT in the context of Shor's algorithm.

4 Numerical experiments

In this section, we will provide numerical illustrations of the theoretical results presented in this work. The algorithms have been implemented in Python 3.8 and added to the toolbox Scikit-TT¹. For comparison purposes, we use Qiskit² [61] for simulating quantum circuits.

4.1 Quantum full adder network

As a first example, we consider a full-adder network. In Section 3.1 we already described how to express a single quantum full adder as an MPO. Due to the structure of the decomposition, we can directly couple several adders in order to construct a quantum full-adder network (QFAN). More precisely, the corresponding MPO representation of the network can be derived by contracting the last core of the previous adder with the first core of the subsequent adder:

$$\begin{aligned} \mathbf{G}_{\text{QFAN}} &= \prod_{i=1}^n I^{\otimes 3(n-i)} \otimes \mathbf{G} \otimes I^{\otimes 3(i-1)} \\ &= \left(I^{\otimes 3(n-1)} \otimes \mathbf{G} \right) \cdot \left(I^{\otimes 3(n-2)} \otimes \mathbf{G} \otimes I^{\otimes 3} \right) \cdot \dots \cdot \left(\mathbf{G} \otimes I^{\otimes 3(n-1)} \right) \\ &= \left[\mathbf{G}^{(1)} \right] \otimes \left[\mathbf{G}^{(2)} \right] \otimes \left[\mathbf{G}^{(3)} \right] \otimes \left[\mathbf{C} \right] \otimes \left[\mathbf{G}^{(2)} \right] \otimes \left[\mathbf{G}^{(3)} \right] \otimes \left[\mathbf{C} \right] \otimes \dots \\ &\quad \dots \otimes \left[\mathbf{C} \right] \otimes \left[\mathbf{G}^{(2)} \right] \otimes \left[\mathbf{G}^{(3)} \right] \otimes \left[\mathbf{G}^{(4)} \right], \end{aligned}$$

where \mathbf{G} denotes the MPO (11) and n is the number of QFAs in the network, i.e., the size of the qubit system is $3n + 1$. The core \mathbf{C} is given by

$$\left[\mathbf{C} \right] = \left[\mathbf{G}_{\text{QFA}}^{(1)} \right] \cdot \left[\mathbf{G}_{\text{QFA}}^{(4)} \right] = \left[\begin{array}{ccc} \sigma_x C_0 & I & \sigma_x C_1 \end{array} \right] \cdot \left[\begin{array}{c} I \\ \sigma_x \end{array} \right] = \left[\begin{array}{ccc} \sigma_x C_0 & I & \sigma_x C_1 \\ C_1 & \sigma_x & C_0 \end{array} \right].$$

Here, \cdot denotes the (core-wise) contraction of corresponding column and row modes. The diagrammatic notation of the quantum full-adder network is shown in Figure 7 (a).

We implement quantum full-adder networks comprising different numbers of full adders and compare our results with the state probabilities computed by Qiskit when measuring the output qubits S_i , $i = 1, \dots, n$, and C_{out} . In order to not only add simple basis states but rather superposition states, we choose the following state as the initial state:

$$\begin{aligned} \Psi &= (I \otimes H \otimes H \otimes I \otimes H \otimes H \otimes I \otimes \dots \otimes I \otimes H \otimes H \otimes I) \cdot |0^{3n+1}\rangle \\ &= \frac{1}{2^n} \begin{bmatrix} 1 \\ 0 \end{bmatrix} \otimes \begin{bmatrix} 1 \\ 1 \end{bmatrix} \otimes \begin{bmatrix} 1 \\ 1 \end{bmatrix} \otimes \begin{bmatrix} 1 \\ 0 \end{bmatrix} \otimes \begin{bmatrix} 1 \\ 1 \end{bmatrix} \otimes \begin{bmatrix} 1 \\ 1 \end{bmatrix} \otimes \begin{bmatrix} 1 \\ 0 \end{bmatrix} \otimes \dots \otimes \begin{bmatrix} 1 \\ 0 \end{bmatrix} \otimes \begin{bmatrix} 1 \\ 1 \end{bmatrix} \otimes \begin{bmatrix} 1 \\ 1 \end{bmatrix} \otimes \begin{bmatrix} 1 \\ 0 \end{bmatrix}, \end{aligned}$$

where Hadamard gates are applied to each of the input qubits $|A_i\rangle$ and $|B_i\rangle$, $i = 1, \dots, n$, cf. Figure 7 (b). For manageable sizes of the QFAN, we are able to directly extract the probability tensor \mathbf{P} from the product $\mathbf{G}_{\text{QFAN}} \Psi$, see Section 2.4. Our experiments confirm that the distributions computed by Qiskit converge to those given by \mathbf{P} (disregarding different orderings) with increasing sample size. See Figure 8 (a) for the probability distribution for $n = 2$. However, since the storage consumption of the probability tensor is $O(2^{n+1})$ in the full format, we employ the sampling strategy described in Section 2.4. In Figure 8 (b), we show the average computation times (including construction and measuring phase) needed for generating 10^5 samples of the output of QFANs with increasing number of full adders.

¹https://github.com/PGelss/scikit_tt

²<https://github.com/Qiskit/qiskit>

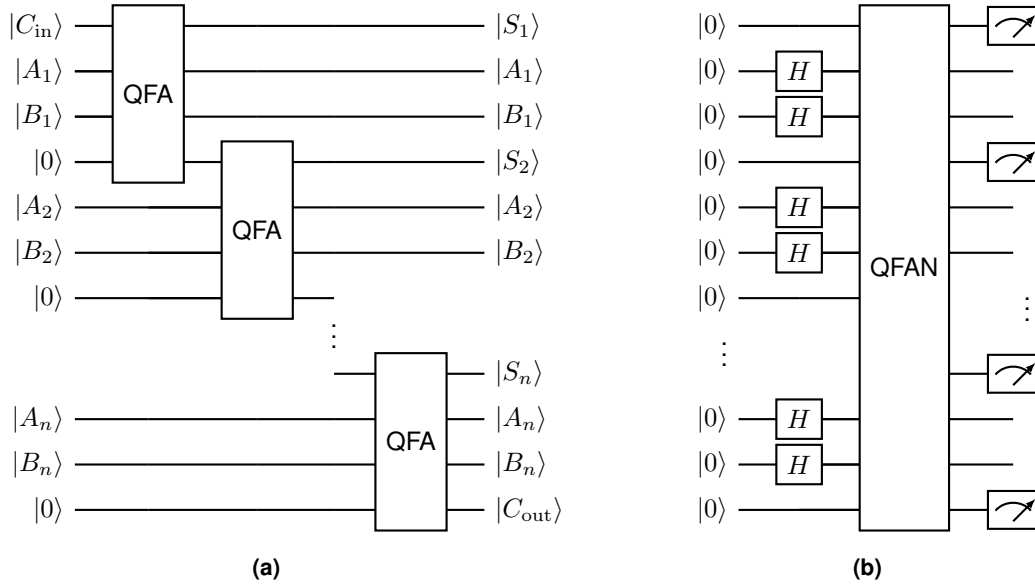


Figure 7: Quantum full-adder network: (a) A QFAN is constructed by successively coupling several QFAs, i.e., by passing the last output qubit of one adder to the first input qubit of another adder. (b) The QFANs simulated in this experiment act on qubit registers of different sizes with a superposition of the inputs for A_i, B_i as initial quantum state.

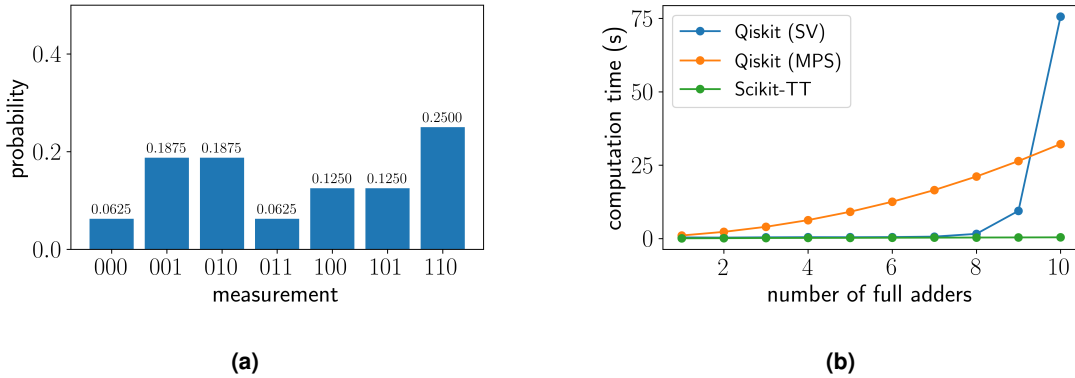


Figure 8: Results of the QFAN simulations: (a) Example of the probability distribution when measuring $|S_1, \dots, S_n, C_{out}\rangle$ for $n = 2$, computed by generative sampling of the final quantum state in MPS format. (b) Average computation times for generating 10^5 samples for different numbers of QFAs using Qiskit (either with the statevector (SV) or MPS simulation method) and Scikit-TT.

For the Qiskit simulations, we use the AerSimulator backend and employ both the statevector as well as the MPS simulation method. That is, similar to our method, Qiskit also uses MPS networks for expressing the quantum states, whereas gate operations on non-consecutive qubits require a series of swap gates applied to the MPS cores to ensure that the respective qubits are adjacent. One can see that, in contrast to the Qiskit statevector simulations, the runtimes of the tensor-based approaches depend only linearly on the number of QFAs. The MPO-based method implemented using Scikit-TT, however, requires significantly less time for constructing and sampling the final quantum state. This example demonstrates the potential of tensor formats for speeding up the sampling phase in quantum system simulations. Moreover, the proposed MPO-based approach may help to mitigate the curse of dimensionality especially when considering circuits on high-dimensional qubit registers. For instance, we can easily simulate a network consisting of 100 QFAs and only need about 30 s for generating 10^6 samples.

4.2 Quantum Fourier transform

As illustrated in the previous section, one of the possible advantages of MPO-based circuit representations is the acceleration of quantum simulations in certain cases. In order to support this claim, let us consider the MPO decomposition of the QFT introduced in Section 3.3. Here, we rely on the decompositions of the gate groups and do not consider a closed MPO representation of the whole circuit at once. In fact, the operators G_i corresponding to the different gate groups all have an MPO rank of 2 (except for G_n which has rank 1) and their contraction would yield a highly-entangled MPO. That is, we simulate the QFT by alternatingly applying an operator G_i (15) and performing an orthonormalization step, see Appendix A.1.2, to control the ranks of the intermediate quantum states. As we already discussed in Section 3.3, every gate group G_i maps to a quantum state which can be represented by a rank-one tensor if the quantum register is initialized to a basis state in the computational basis. For the following experiment, we therefore randomly choose initial quantum states from the computational basis while increasing the size of the qubit system and compare Scikit-TT with Qiskit simulations using the built-in MPS simulation method. The results of the different quantum circuit simulations in terms of computation times for generating $s = 10^2, 10^4, 10^6$ samples are shown in Table 1.

Table 1: Results of QFT simulations: For different numbers of qubits n and samples s , the average execution times (in seconds) and corresponding standard deviations of the Qiskit and Scikit-TT simulations are shown. For each parameter choice, the simulations were repeated 100 times with randomly drawn basis states as inputs.

		$n = 16$	$n = 32$	$n = 64$	$n = 128$
Qiskit	$s = 10^2$	0.07 ± 0.08	0.12 ± 0.02	0.33 ± 0.05	1.09 ± 0.11
	$s = 10^4$	0.16 ± 0.01	0.27 ± 0.03	0.57 ± 0.05	1.57 ± 0.10
	$s = 10^6$	6.65 ± 0.03	15.12 ± 0.05	25.72 ± 0.10	48.35 ± 0.11
Scikit-TT	$s = 10^2$	0.04 ± 0.00	0.15 ± 0.00	0.59 ± 0.00	2.31 ± 0.01
	$s = 10^4$	0.07 ± 0.00	0.20 ± 0.00	0.66 ± 0.00	2.43 ± 0.01
	$s = 10^6$	5.34 ± 0.15	7.82 ± 0.18	11.51 ± 0.16	20.39 ± 0.20

While the computation time of Qiskit grows (almost) linearly with the size of the qubit system, the scaling behavior of the MPO approach changes with increasing number of samples. This can be explained by the low-rank MPS/MPO representations of the quantum states and gate groups: In addition to the sampling procedure, the dominant operations in our simulations are the orthonormalization procedures, i.e., applying sequences of n SVDs to every MPS decomposition of the n intermediate states, see Appendix A.1.2. Since the ranks of every gate group operator and, therefore, every intermediate quantum state are bounded by 2, the computational complexity of the construction of the final quantum state can be estimated as $O(8n^2)$. For the sampling procedure, we can estimate the computational costs as $O(8sn)$, cf. Section 2.4. That is, the complexity is mainly determined by the construction and orthonormalization of the wave functions in MPS format for a small number of samples and, thus, increases quadratically with the number of qubits. On the other hand, the computation times show a linearly scaling with the system size when we consider larger numbers of samples because the computational complexity of the sampling scheme outweighs that of the orthonormalization steps. For high-dimensional qubit systems, in particular, a large number of required measurements is a common bottleneck of many quantum algorithms. Thus, MPO/MPS-based formulations not only offer an alternative way of treating quantum circuits but may also accelerate the simulation of these if the final quantum state has sufficiently low MPS ranks.

4.3 Shor’s algorithm

Shor’s algorithm [3] was one of the first quantum algorithms that provided a significant advantage over classical computations. Given an integer M , the goal is to find a non-trivial divisor by combining classical and quantum computations. The computational complexity of Shor’s algorithm is $O((\log M)^3)$, demonstrating an almost exponential acceleration compared to best-known classical factorization algorithms. Therefore, Shor’s algorithms might be used to break RSA encryption [62]—which is based

on composite numbers having two large prime factors—much faster than in the classical case. The classical part of Shor’s algorithm is to find a number a that has no common divisor with a given composite number M , whereas the quantum part exploits the inverse QFT on a $2n$ -qubit register with $N = 2^n > M$, see Section 3.3, for finding the period p of the function $f(x) = a^x \bmod M$ in polynomial time. The structure of Shor’s algorithm can be summarized by the following essential stages:

- 1) Choose $1 < a < M$ randomly. If a and M are coprime, go to step 2, otherwise $\gcd(a, M)$ is a nontrivial factor of M .
- 2) Initialize the input register with $2n$ qubits and the target register with n qubits, both to the zero state. Apply Hadamard gates to the qubits in the input register, the modular exponentiation circuit U_f to both registers and afterwards the inverse QFT to the input register. When measuring the input register, we obtain a (basis) state $|y\rangle$.
- 3) Calculate candidates for the period p from y , see below. If all candidates fail, go back to step 2.
- 4) If p is odd or $a^{p/2} \equiv -1 \pmod{N}$, got back to step 1. Otherwise, either $\gcd(a^{p/2} - 1, M)$ or $\gcd(a^{p/2} + 1, M)$ is a nontrivial factor of M .

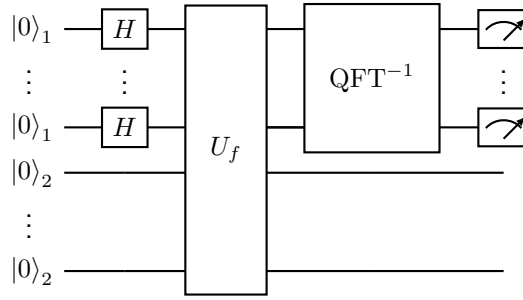


Figure 9: Shor’s algorithm: The input register (marked by the subscript 1) holds the superposition of the basis states $|0\rangle, \dots, |N^2 - 1\rangle$, while the output register (marked the by subscript 2) holds the superposition of the values of f after application of U_f . The inverse QFT is applied to the first register to estimate the phase of U_f .

Figure 9 shows the corresponding quantum circuit. The first step, computing the greatest common divisor of a and M , can be simply performed by using the Euclidean algorithm. The modular exponentiation circuit U_f in the second step represents the function f in the sense that the quantum state after the application of the Hadamard gates and U_f is

$$U_f \left(\frac{1}{N} \sum_{x=0}^{N^2-1} |x, 0^n\rangle \right) = \frac{1}{N} \sum_{x=0}^{N-1} |x, f(x)\rangle. \quad (16)$$

Applying the inverse QFT to the first register leads to the quantum state

$$\text{QFT}^{-1} \left(\frac{1}{N} \sum_{x=0}^{N^2-1} |x, f(x)\rangle \right) = \frac{1}{N^2} \sum_{x=0}^{N^2-1} \sum_{y=0}^{N^2-1} e^{-\frac{2\pi i}{N^2} xy} |y, f(x)\rangle.$$

Supposing we finally obtain a state $|y\rangle$ when measuring the first register, we can use continued fraction expansion on a classical computer to find approximations z/q of y/N , where q is equal to the period p or at least a factor of it with high probability. For a more detailed description of the different steps of Shor’s algorithm, we refer to [50]. The construction of U_f is the most challenging part when implementing Shor’s algorithm. It is usually based on controlled modular multiplier blocks, individually designed for each choice of a and M [63, 64]. In terms of tensor products, however, we can construct an explicit

representation for any base and modulus. That is, with respect to the above circuit, the tensor operator corresponding to (16) is given by

$$\begin{aligned} \mathbf{U}_f &= \sum_{x=0}^{N^2-1} C_{x_1} \otimes \cdots \otimes C_{x_{2n}} \otimes \sigma_x^{f(x)_1} \otimes \cdots \otimes \sigma_x^{f(x)_n} \\ &= \sum_{z=0}^{N-1} \left(\sum_{\substack{x=1 \\ f(x)=z}}^{N^2-1} C_{x_1} \otimes \cdots \otimes C_{x_{2n}} \right) \otimes \sigma_x^{z_1} \otimes \cdots \otimes \sigma_x^{z_n}, \end{aligned}$$

where we again define $C_0 = I - C$ and $C_1 = C$.

Let us consider the case of $M = 15$ and $a \in \{2, 4, 7, 8, 11, 13\}$. That is, our input register has 8 and the target register 4 qubits. In fact, the operator \mathbf{U}_f corresponding to any choice of a can be represented as an MPO with either rank 2 or 4, which is a direct consequence of the multiplicative orders of the different bases. The explicit decompositions are given by

$$\begin{aligned} a = 2: \quad \mathbf{U}_f &= I^{\otimes 6} \otimes C_0 \otimes C_0 \otimes I \otimes I \otimes I \otimes \sigma_x \\ &\quad + I^{\otimes 6} \otimes C_0 \otimes C_1 \otimes I \otimes I \otimes \sigma_x \otimes I \\ &\quad + I^{\otimes 6} \otimes C_1 \otimes C_0 \otimes I \otimes \sigma_x \otimes I \otimes I \\ &\quad + I^{\otimes 6} \otimes C_1 \otimes C_1 \otimes \sigma_x \otimes I \otimes I \otimes I, \\ a = 4: \quad \mathbf{U}_f &= I^{\otimes 6} \otimes I \otimes C_0 \otimes I \otimes I \otimes I \otimes \sigma_x \\ &\quad + I^{\otimes 6} \otimes I \otimes C_1 \otimes I \otimes \sigma_x \otimes I \otimes I, \\ a = 7: \quad \mathbf{U}_f &= I^{\otimes 6} \otimes C_0 \otimes C_0 \otimes I \otimes I \otimes I \otimes \sigma_x \\ &\quad + I^{\otimes 6} \otimes C_0 \otimes C_1 \otimes I \otimes \sigma_x \otimes \sigma_x \otimes \sigma_x \\ &\quad + I^{\otimes 6} \otimes C_1 \otimes C_0 \otimes I \otimes \sigma_x \otimes I \otimes I \\ &\quad + I^{\otimes 6} \otimes C_1 \otimes C_1 \otimes \sigma_x \otimes \sigma_x \otimes I \otimes \sigma_x, \\ a = 8: \quad \mathbf{U}_f &= I^{\otimes 6} \otimes C_0 \otimes C_0 \otimes I \otimes I \otimes I \otimes \sigma_x \\ &\quad + I^{\otimes 6} \otimes C_0 \otimes C_1 \otimes \sigma_x \otimes I \otimes I \otimes I \\ &\quad + I^{\otimes 6} \otimes C_1 \otimes C_0 \otimes I \otimes \sigma_x \otimes I \otimes I \\ &\quad + I^{\otimes 6} \otimes C_1 \otimes C_1 \otimes I \otimes I \otimes \sigma_x \otimes I, \\ a = 11: \quad \mathbf{U}_f &= I^{\otimes 6} \otimes I \otimes C_0 \otimes I \otimes I \otimes I \otimes \sigma_x \\ &\quad + I^{\otimes 6} \otimes I \otimes C_1 \otimes \sigma_x \otimes I \otimes \sigma_x \otimes \sigma_x, \\ a = 13: \quad \mathbf{U}_f &= I^{\otimes 6} \otimes C_0 \otimes C_0 \otimes I \otimes I \otimes I \otimes \sigma_x \\ &\quad + I^{\otimes 6} \otimes C_0 \otimes C_1 \otimes \sigma_x \otimes \sigma_x \otimes I \otimes \sigma_x \\ &\quad + I^{\otimes 6} \otimes C_1 \otimes C_0 \otimes I \otimes \sigma_x \otimes I \otimes I \\ &\quad + I^{\otimes 6} \otimes C_1 \otimes C_1 \otimes I \otimes \sigma_x \otimes \sigma_x \otimes \sigma_x, \\ a = 14: \quad \mathbf{U}_f &= I^{\otimes 6} \otimes I \otimes C_0 \otimes I \otimes I \otimes I \otimes \sigma_x \\ &\quad + I^{\otimes 6} \otimes I \otimes C_1 \otimes \sigma_x \otimes \sigma_x \otimes \sigma_x \otimes I. \end{aligned}$$

Thus, we can represent Shor's algorithm by a sequence of MPOs comprising a superpositioning operator, the operator \mathbf{U}_f , and the gate groups of the inverse QFT, see Section 3.3. Note that the quantum state after the application the first two MPOs is given by

$$\mathbf{U}_f (H^{\otimes 2n} \otimes I^{\otimes n}) |0^{2n}, 0^n\rangle = \frac{1}{2^n} \mathbf{U}_f \cdot \left(\begin{bmatrix} 1 \\ 1 \end{bmatrix} \otimes \cdots \otimes \begin{bmatrix} 1 \\ 1 \end{bmatrix} \otimes \begin{bmatrix} 1 \\ 0 \end{bmatrix} \otimes \cdots \otimes \begin{bmatrix} 1 \\ 0 \end{bmatrix} \right)$$

and, therefore, has the same ranks (at most) as \mathbf{U}_f . As in the previous section, we orthonormalize the intermediate quantum states to reduce the ranks between the applications of the gate groups of the inverse QFT, see Appendix A.1.2. Lastly, we construct the probability tensor as described in Section 2.4. Reading the measured bitstrings in reversed order (due to the omission of SWAP operations), we then find for each choice of a that the results shown in Table 2 are exactly the same as when using the Qiskit implementation described in [65].

The results show that it is possible to construct low-rank decompositions for even more complex quantum algorithms. Although we here do not focus on an explicit representation of the entire circuit,

Table 2: Results of Shor’s factorization algorithm for $M = 15$: The possible bases can be divided in two groups. For $a \in \{2, 7, 8, 13\}$, the final quantum state (before measuring) has rank $r = 4$ and the measured basis state indices remain the same for each a . If $a \in \{4, 11, 14\}$, then the final quantum state can be represented by a rank-2 MPS. For both groups, the extracted period and the corresponding prime factors are shown. If $y = 0$ is measured, Shor’s algorithm fails and returns no factors of M .

base a	rank r	measurement y	period q	factors (M_1, M_2)
2, 7, 8, 13	4	0	1	\emptyset
		64	4	(3, 5)
		128	2	(3, 1)
		192	4	(3, 5)
4, 11, 14	2	0	1	\emptyset
		128	2	(3, 1)

we can directly simulate its action on the qubit register while keeping the ranks of the intermediate quantum states low. The ranks of the final quantum state in this case reflect the order of the associated base.

5 Conclusion and outlook

In this paper, we used the MPO format to express quantum algorithms in a tensor-based form. In particular, we have shown how to systematically decompose quantum gates acting on arbitrary qubits. With the aid of various benchmark problems, we discussed tensor-based representations of quantum circuits by contracting several MPO decompositions corresponding to different types of quantum logic gates. We showed that it is possible to derive compact MPO networks of various quantum circuits with ranks much smaller than the theoretical bounds allowing for direct ways of interpretation in terms of entanglement structure and their action on different basis states.

Our numerical experiments showed convincingly that the MPO-based construction of quantum algorithms is not only equivalent in terms of simulation results but also may allow us to speed up computations by exploiting the coupling structure of low-rank tensor decompositions. So far, we only investigated ideal quantum simulations, i.e., neither concepts like error correction nor fault tolerance are considered in this work. However, future research will include the investigation of quantum algorithms for both ideal quantum computers and noisy devices.

The presented results are an important step towards the MPO-based construction and analysis of quantum circuits, which paves the way for exploring new techniques for developing algorithms. As MPSs are a natural way of describing quantum states, we showed that MPOs can efficiently be used in the same fashion for representing quantum circuits in a closed form and demonstrated a new framework for designing and simulating complex quantum circuits. Therefore, future studies will particularly focus on the conversion between MPO decompositions and quantum circuit representations using sets of universal gates.

Acknowledgments

This research has been funded by the Deutsche Forschungsgemeinschaft (CRC 1114, “Scaling Cascades in Complex Systems”).

References

- [1] F. Arute, K. Arya, R. Babbush, D. Bacon, J. C. Bardin, R. Barends, R. Biswas, S. Boixo, F. G. S. L. Brandao, D. A. Buell, B. Burkett, Y. Chen, and Z. Chen. “Quantum supremacy using a programmable superconducting processor”. In: *Nature* 574 (2019), pp. 505–510. doi: [10.1038/s41586-019-1666-5](https://doi.org/10.1038/s41586-019-1666-5).

- [2] R. P. Feynman. “Simulating physics with computers”. In: *International Journal of Theoretical Physics* 21 (6 1982), pp. 467–488. DOI: [10.1007/BF02650179](https://doi.org/10.1007/BF02650179).
- [3] P. W. Shor. “Algorithms for quantum computation: Discrete logarithms and factoring”. In: *Proceedings 35th Annual Symposium on Foundations of Computer Science*. 1994, pp. 124–134. DOI: [10.1109/SFCS.1994.365700](https://doi.org/10.1109/SFCS.1994.365700).
- [4] L. K. Grover. “A fast quantum mechanical algorithm for database search”. In: *Proceedings of the Twenty-Eighth Annual ACM Symposium on Theory of Computing*. STOC '96. Philadelphia, Pennsylvania, USA: Association for Computing Machinery, 1996, pp. 212–219. DOI: [10.1145/237814.237866](https://doi.org/10.1145/237814.237866).
- [5] D. R. Simon. “On the power of quantum computation”. In: *SIAM Journal on Computing* 26.5 (1997), pp. 1474–1483. DOI: [10.1137/S0097539796298637](https://doi.org/10.1137/S0097539796298637).
- [6] P. Rebentrost, B. Gupt, and T. R. Bromley. “Quantum computational finance: Monte Carlo pricing of financial derivatives”. In: *Phys. Rev. A* 98 (2 2018), p. 022321. DOI: [10.1103/PhysRevA.98.022321](https://doi.org/10.1103/PhysRevA.98.022321).
- [7] B. Coyle, M. Henderson, J. C. J. Le, N. Kumar, M. Paini, and E. Kashefi. “Quantum versus classical generative modelling in finance”. In: *Quantum Science and Technology* 6.2 (2021), p. 024013. DOI: [10.1088/2058-9565/abd3db](https://doi.org/10.1088/2058-9565/abd3db).
- [8] D. J. Bernstein and T. Lange. “Post-quantum cryptography”. In: *Nature* 549 (7671 2017), pp. 188–194. DOI: [10.1038/nature23461](https://doi.org/10.1038/nature23461).
- [9] S. Pirandola et al. “Advances in quantum cryptography”. In: *Advances in Optics and Photonics* 12.4 (2020), pp. 1012–1236. DOI: [10.1364/AOP.361502](https://doi.org/10.1364/AOP.361502).
- [10] I. Kassal, S. P. Jordan, P. J. Love, M. Mohseni, and A. Aspuru-Guzik. “Polynomial-time quantum algorithm for the simulation of chemical dynamics”. In: *Proceedings of the National Academy of Sciences* 105.48 (2008), pp. 18681–18686. DOI: [10.1073/pnas.0808245105](https://doi.org/10.1073/pnas.0808245105).
- [11] S. McArdle, S. Endo, A. Aspuru-Guzik, S. C. Benjamin, and X. Yuan. “Quantum computational chemistry”. In: *Rev. Mod. Phys.* 92 (1 2020), p. 015003. DOI: [10.1103/RevModPhys.92.015003](https://doi.org/10.1103/RevModPhys.92.015003).
- [12] J. Biamonte, P. Wittek, N. Pancotti, P. Rebentrost, N. Wiebe, and S. Lloyd. “Quantum machine learning”. In: *Nature* 549.7671 (2017), pp. 195–202. DOI: [10.1038/nature23474](https://doi.org/10.1038/nature23474).
- [13] Y. Zhang and Q. Ni. “Recent advances in quantum machine learning”. In: *Quantum Engineering* 2.1 (2020), e34. DOI: <https://doi.org/10.1002/que2.34>.
- [14] C. Monroe, R. Raussendorf, A. Ruthven, K. R. Brown, P. Maunz, L.-M. Duan, and J. Kim. “Large-scale modular quantum-computer architecture with atomic memory and photonic interconnects”. In: *Phys. Rev. A* 89 (2 2014), p. 022317. DOI: [10.1103/PhysRevA.89.022317](https://doi.org/10.1103/PhysRevA.89.022317).
- [15] M. Saffman. “Quantum computing with atomic qubits and Rydberg interactions: Progress and challenges”. In: *Journal of Physics B: Atomic, Molecular and Optical Physics* 49.20 (2016), p. 202001. DOI: [10.1088/0953-4075/49/20/202001](https://doi.org/10.1088/0953-4075/49/20/202001).
- [16] A. Gaita-Ariño, F. Luis, S. Hill, and E. Coronado. “Molecular spins for quantum computation”. In: *Nature Chemistry* 11 (4 2019), pp. 301–309. DOI: [10.1038/s41557-019-0232-y](https://doi.org/10.1038/s41557-019-0232-y).
- [17] H.-S. Zhong et al. “Quantum computational advantage using photons”. In: *Science* 370.6523 (2020), pp. 1460–1463. DOI: [10.1126/science.abe8770](https://doi.org/10.1126/science.abe8770).
- [18] J. Clarke and F. K. Wilhelm. “Superconducting quantum bits”. In: *Nature* 453.7198 (2008), pp. 1031–1042. DOI: [10.1038/nature07128](https://doi.org/10.1038/nature07128).
- [19] L. Spector. *Automatic Quantum Computer Programming: A Genetic Programming Approach (Genetic Programming)*. Boston, MA: Springer, 2004. DOI: [10.1007/b116136](https://doi.org/10.1007/b116136).
- [20] V. M. Kendon. “A random walk approach to quantum algorithms”. In: *Philosophical Transactions of the Royal Society A: Mathematical, Physical and Engineering Sciences* 364.1849 (2006), pp. 3407–3422. DOI: [10.1098/rsta.2006.1901](https://doi.org/10.1098/rsta.2006.1901).
- [21] M. C. Bañuls, R. Orús, J. I. Latorre, A. Pérez, and P. Ruiz-Femenia. “Simulation of many-qubit quantum computation with matrix product states”. In: *Phys. Rev. A* 73 (2 2006), p. 022344. DOI: [10.1103/PhysRevA.73.022344](https://doi.org/10.1103/PhysRevA.73.022344).

- [22] B. P. Lanyon, C. Maier, M. Holzäpfel, T. Baumgratz, C. Hempel, P. Jurcevic, I. Dhand, A. S. Buyskikh, A. J. Daley, M. Cramer, M. B. Plenio, R. Blatt, and C. F. Roos. “Efficient tomography of a quantum many-body system”. In: *Nature Physics* 13 (12 2017), pp. 1158–1162. DOI: [10.1038/nphys4244](https://doi.org/10.1038/nphys4244).
- [23] M. Ganahl, J. Rincón, and G. Vidal. “Continuous matrix product states for quantum fields: An energy minimization algorithm”. In: *Phys. Rev. Lett.* 118 (22 2017), p. 220402. DOI: [10.1103/PhysRevLett.118.220402](https://doi.org/10.1103/PhysRevLett.118.220402).
- [24] S. De Nicola, A. A. Michailidis, and M. Serbyn. “Entanglement view of dynamical quantum phase transitions”. In: *Phys. Rev. Lett.* 126 (4 2021), p. 040602. DOI: [10.1103/PhysRevLett.126.040602](https://doi.org/10.1103/PhysRevLett.126.040602).
- [25] Y. Zhou, E. M. Stoudenmire, and X. Waintal. “What limits the simulation of quantum computers?” In: *Phys. Rev. X* 10 (4 2020), p. 041038. DOI: [10.1103/PhysRevX.10.041038](https://doi.org/10.1103/PhysRevX.10.041038).
- [26] C. Guo, Y. Liu, M. Xiong, S. Xue, X. Fu, A. Huang, X. Qiang, P. Xu, J. Liu, S. Zheng, H.-L. Huang, M. Deng, D. Poletti, W.-S. Bao, and J. Wu. “General-purpose quantum circuit simulator with projected entangled-pair states and the quantum supremacy frontier”. In: *Phys. Rev. Lett.* 123 (19 2019), p. 190501. DOI: [10.1103/PhysRevLett.123.190501](https://doi.org/10.1103/PhysRevLett.123.190501).
- [27] I. A. Luchnikov, A. V. Berezutskii, and A. K. Fedorov. “Simulating quantum circuits using the multi-scale entanglement renormalization ansatz”. In: *arXiv* (2021). DOI: [10.48550/ARXIV.2112.14046](https://doi.org/10.48550/ARXIV.2112.14046).
- [28] I. Affleck, T. Kennedy, E. H. Lieb, and H. Tasaki. “Rigorous results on valence-bond ground states in antiferromagnets”. In: *Physical Review Letters* 59.7 (1987), pp. 799–802. DOI: [10.1103/PhysRevLett.59.799](https://doi.org/10.1103/PhysRevLett.59.799).
- [29] I. V. Oseledets. “A new tensor decomposition”. In: *Doklady Mathematics* 80.1 (2009), pp. 495–496. DOI: [10.1134/S1064562409040115](https://doi.org/10.1134/S1064562409040115).
- [30] I. V. Oseledets and E. E. Tyrtshnikov. “Breaking the curse of dimensionality, or how to use SVD in many dimensions”. In: *SIAM Journal on Scientific Computing* 31.5 (2009), pp. 3744–3759. DOI: [10.1137/090748330](https://doi.org/10.1137/090748330).
- [31] A. Veit and L. R. Scott. “Using the Tensor-Train Approach to Solve the Ground-State Eigenproblem for Hydrogen Molecules”. In: *SIAM Journal on Scientific Computing* 39.1 (2017), B190–B220. DOI: [10.1137/15M102808X](https://doi.org/10.1137/15M102808X).
- [32] P. Gelß, R. Klein, S. Matera, and B. Schmidt. “Solving the time-independent Schrödinger equation for chains of coupled excitons and phonons using tensor trains”. In: *The Journal of Chemical Physics* 156.2 (2022), p. 024109. DOI: [10.1063/5.0074948](https://doi.org/10.1063/5.0074948).
- [33] S. Klus, P. Gelß, S. Peitz, and C. Schütte. “Tensor-based dynamic mode decomposition”. In: *Nonlinearity* 31.7 (2018), pp. 3359–3380. DOI: [10.1088/1361-6544/aabc8f](https://doi.org/10.1088/1361-6544/aabc8f).
- [34] A. Goeßmann, M. Götte, I. Roth, R. Sweke, G. Kutyniok, and J. Eisert. “Tensor network approaches for learning non-linear dynamical laws”. In: *arXiv* (2020). DOI: [10.48550/ARXIV.2002.12388](https://doi.org/10.48550/ARXIV.2002.12388).
- [35] W. Huggins, P. Patil, B. Mitchell, K. B. Whaley, and E. M. Stoudenmire. “Towards quantum machine learning with tensor networks”. In: *Quantum Science and Technology* 4.2 (2019), p. 024001. DOI: [10.1088/2058-9565/aaea94](https://doi.org/10.1088/2058-9565/aaea94). URL: <https://doi.org/10.1088/2058-9565/aaea94>.
- [36] L. Grasedyck and S. Krämer. “Stable ALS approximation in the TT-format for rank-adaptive tensor completion”. In: *Numerische Mathematik* 143 (4 2019), pp. 855–904. DOI: [10.1007/s00211-019-01072-4](https://doi.org/10.1007/s00211-019-01072-4).
- [37] S. Klus and P. Gelß. “Tensor-based algorithms for image classification”. In: *Algorithms* 12.11 (2019). DOI: [10.3390/a12110240](https://doi.org/10.3390/a12110240).
- [38] P. Gelß, S. Klus, J. Eisert, and C. Schütte. “Multidimensional approximation of nonlinear dynamical systems”. In: *Journal of Computational and Nonlinear Dynamics* 14.6 (2019), p. 061006. DOI: [10.1115/1.4043148](https://doi.org/10.1115/1.4043148).

- [39] F. Nüske, P. Gelß, S. Klus, and C. Clementi. “Tensor-based computation of metastable and coherent sets”. In: *Physica D: Nonlinear Phenomena* 427 (2021), p. 133018. DOI: [10.1016/j.physd.2021.133018](https://doi.org/10.1016/j.physd.2021.133018).
- [40] M. Lücke and F. Nüske. “tgEDMD: Approximation of the Kolmogorov operator in tensor train format”. In: *arXiv* (2021). DOI: [10.48550/ARXIV.2111.09606](https://doi.org/10.48550/ARXIV.2111.09606).
- [41] S.-J. Ran. “Encoding of matrix product states into quantum circuits of one- and two-qubit gates”. In: *Phys. Rev. A* 101 (3 2020), p. 032310. DOI: [10.1103/PhysRevA.101.032310](https://doi.org/10.1103/PhysRevA.101.032310).
- [42] G. Torlai, C. J. Wood, A. Acharya, G. Carleo, J. Carrasquilla, and L. Aolita. “Quantum process tomography with unsupervised learning and tensor networks”. In: *arXiv* (2020). DOI: [10.48550/ARXIV.2006.02424](https://doi.org/10.48550/ARXIV.2006.02424).
- [43] C. G. Almudever, L. Lao, X. Fu, N. Khammassi, I. Ashraf, D. Iorga, S. Varsamopoulos, C. Eichler, A. Wallraff, L. Geck, A. Kruth, J. Knoch, H. Bluhm, and K. Bertels. “The engineering challenges in quantum computing”. In: *Design, Automation & Test in Europe Conference & Exhibition (DATE), 2017*. 2017, pp. 836–845. DOI: [10.23919/DATE.2017.7927104](https://doi.org/10.23919/DATE.2017.7927104).
- [44] A. J. Ferris and G. Vidal. “Perfect sampling with unitary tensor networks”. In: *Phys. Rev. B* 85 (16 2012), p. 165146. DOI: [10.1103/PhysRevB.85.165146](https://doi.org/10.1103/PhysRevB.85.165146).
- [45] Z.-Y. Han, J. Wang, H. Fan, L. Wang, and P. Zhang. “Unsupervised generative modeling using matrix product states”. In: *Phys. Rev. X* 8 (3 2018), p. 031012. DOI: [10.1103/PhysRevX.8.031012](https://doi.org/10.1103/PhysRevX.8.031012).
- [46] J. S. Bell. “On the Einstein Podolsky Rosen paradox”. In: *Physics Physique Fizika* 1 (3 1964), pp. 195–200. DOI: [10.1103/PhysicsPhysiqueFizika.1.195](https://doi.org/10.1103/PhysicsPhysiqueFizika.1.195).
- [47] D. M. Greenberger, M. A. Horne, and A. Zeilinger. “Going beyond Bell’s theorem”. In: *Bell’s Theorem, Quantum Theory and Conceptions of the Universe*. Ed. by M. Kafatos. Vol. 37. Fundamental Theories of Physics. Dordrecht: Springer, 1989, pp. 69–72. DOI: [10.1007/978-94-017-0849-4_10](https://doi.org/10.1007/978-94-017-0849-4_10).
- [48] W. Dür, G. Vidal, and J. I. Cirac. “Three qubits can be entangled in two inequivalent ways”. In: *Phys. Rev. A* 62 (6 2000), p. 062314. DOI: [10.1103/PhysRevA.62.062314](https://doi.org/10.1103/PhysRevA.62.062314).
- [49] A. Barenco, C. H. Bennett, R. Cleve, D. P. DiVincenzo, N. Margolus, P. Shor, T. Sleator, J. A. Smolin, and H. Weinfurter. “Elementary gates for quantum computation”. In: *Phys. Rev. A* 52 (5 1995), pp. 3457–3467. DOI: [10.1103/PhysRevA.52.3457](https://doi.org/10.1103/PhysRevA.52.3457).
- [50] M. A. Nielsen and I. L. Chuang. *Quantum computation and quantum information: 10th anniversary edition*. Cambridge University Press, 2010. DOI: [10.1017/CB09780511976667](https://doi.org/10.1017/CB09780511976667).
- [51] D. S. Wang, C. D. Hill, and L. C. Hollenberg. “Simulations of Shor’s algorithm using matrix product states”. In: 16.7 (2017), pp. 1–13. DOI: [10.1007/s11128-017-1587-x](https://doi.org/10.1007/s11128-017-1587-x).
- [52] V. Kazeev, O. Reichmann, and C. Schwab. “Low-rank tensor structure of linear diffusion operators in the TT and QTT formats”. In: *Linear Algebra and its Applications* 438.11 (2013), pp. 4204–4221. DOI: [10.1016/j.laa.2013.01.009](https://doi.org/10.1016/j.laa.2013.01.009).
- [53] S. Keller, M. Dolfi, M. Troyer, and M. Reiher. “An efficient matrix product operator representation of the quantum chemical Hamiltonian”. In: *The Journal of Chemical Physics* 143.24 (2015), p. 244118. DOI: [10.1063/1.4939000](https://doi.org/10.1063/1.4939000).
- [54] P. Gelß, S. Klus, S. Matera, and C. Schütte. “Nearest-neighbor interaction systems in the tensor-train format”. In: *Journal of Computational Physics* 341 (2017), pp. 140–162. DOI: [10.1016/j.jcp.2017.04.007](https://doi.org/10.1016/j.jcp.2017.04.007).
- [55] R. P. Feynman. “Quantum mechanical computers”. In: *Foundations of Physics* 16 (6 1986), pp. 507–531. DOI: [10.1103/PhysRevB.85.165146](https://doi.org/10.1103/PhysRevB.85.165146).
- [56] N. Johansson and J.-Å. Larsson. “Efficient classical simulation of the Deutsch-Jozsa and Simon’s algorithms”. In: *Quantum Information Processing* 16 (9 2017), p. 233. DOI: [10.1007/s11128-017-1679-7](https://doi.org/10.1007/s11128-017-1679-7).
- [57] T. Santoli and C. Schaffner. “Using Simon’s algorithm to attack symmetric-key cryptographic primitives”. In: *Quantum Info. Comput.* 17.1–2 (2017), pp. 65–78.

- [58] K. Shinagawa and T. Iwata. “Quantum attacks on sum of Even-Mansour pseudorandom functions”. In: *Information Processing Letters* 173 (2022), p. 106172. DOI: [10.1016/j.ipl.2021.106172](https://doi.org/10.1016/j.ipl.2021.106172).
- [59] D. Coppersmith. “An approximate Fourier transform useful in quantum factoring”. In: *IBM Research Report* (1994), RC-19642.
- [60] D. Camps, R. Van Beeumen, and C. Yang. “Quantum Fourier transform revisited”. In: *Numerical Linear Algebra with Applications* 28.1 (2021), e2331. DOI: [10.1002/nla.2331](https://doi.org/10.1002/nla.2331).
- [61] S. Anis et al. *Qiskit: An open-source framework for quantum computing*. 2021. DOI: [10.5281/zenodo.2573505](https://doi.org/10.5281/zenodo.2573505).
- [62] C. Gidney and M. Ekerå. “How to factor 2048 bit RSA integers in 8 hours using 20 million noisy qubits”. In: *Quantum* 5 (2021), p. 433. DOI: [10.22331/q-2021-04-15-433](https://doi.org/10.22331/q-2021-04-15-433).
- [63] A. Pavlidis and D. Gizopoulos. “Fast quantum modular exponentiation architecture for Shor’s factoring algorithm”. In: *Quantum Information & Computation* 14.7 & 8 (2014), pp. 649–682.
- [64] Z.-C. Duan, J.-P. Li, J. Qin, Y. Yu, Y.-H. Huo, S. Höfling, C.-Y. Lu, N.-L. Liu, K. Chen, and J.-W. Pan. “Proof-of-principle demonstration of compiled Shor’s algorithm using a quantum dot single-photon source”. In: *Optics Express* 28.13 (2020), pp. 18917–18930. DOI: [10.1364/OE.390209](https://doi.org/10.1364/OE.390209).
- [65] A. Abbas et al. *Learn quantum computation using Qiskit*. 2020. URL: <http://community.qiskit.org/textbook>.

A Appendix

A.1 Construction and manipulation of MPO cores

A.1.1 Linear transformations of MPS cores

Given an MPS core $\mathbf{T}^{(i)} \in \mathbb{C}^{r_{i-1} \times d_i \times r_i}$ as defined in (7), applying a linear transformation represented by the matrix $Q \in \mathbb{C}^{r_i \times \tilde{r}_i}$ from the right results in a new core $\mathbf{U}^{(i)} \in \mathbb{C}^{r_{i-1} \times d_i \times \tilde{r}_i}$, i.e.,

$$\llbracket \mathbf{U}^{(i)} \rrbracket = \llbracket \mathbf{T}^{(i)} \rrbracket \cdot Q = \llbracket \mathbf{T}^{(i)} \rrbracket \cdot \begin{bmatrix} Q_{1,1} & \cdots & Q_{1,\tilde{r}_i} \\ \vdots & \ddots & \vdots \\ Q_{r_i,1} & \cdots & Q_{r_i,\tilde{r}_i} \end{bmatrix}, \quad (17)$$

where each core entry of $\mathbf{U}^{(i)}$ is given by

$$U_{k,x,\ell}^{(i)} = \sum_{\mu=1}^{r_i} T_{k,x,\mu}^{(i)} Q_{\mu,\ell}.$$

That is, the notation in (17) is an alternative way of expressing TT cores defined by the relation

$$U_{:,x,:}^{(i)} = T_{:,x,:}^{(i)} \cdot Q$$

for $x \in \{1, \dots, d_i\}$. The left-multiplication of a matrix $Q \in \mathbb{C}^{\tilde{r}_{i-1} \times r_{i-1}}$ and a TT core and the core manipulation of MPOs are defined analogously. For two TT cores $\mathbf{T}^{(i)} \in \mathbb{C}^{r_{i-1} \times d_i \times r_i}$, $\mathbf{T}^{(i+1)} \in \mathbb{C}^{\tilde{r}_i \times d_{i+1} \times r_{i+1}}$ and a matrix $Q \in \mathbb{C}^{r_i \times \tilde{r}_i}$, it holds that

$$\left(\llbracket \mathbf{T}^{(i)} \rrbracket \cdot Q \right) \otimes \llbracket \mathbf{T}^{(i+1)} \rrbracket = \llbracket \mathbf{T}^{(i)} \rrbracket \otimes \left(Q \cdot \llbracket \mathbf{T}^{(i+1)} \rrbracket \right). \quad (18)$$

This can be directly shown by considering the representation of a single entry of an MPS, see (5).

A.1.2 Orthonormalization of tensors in MPS format

The left- and right-unfoldings of an MPS core $\mathbf{T}^{(i)}$ are given by the matrices $\mathcal{L} \in \mathbb{C}^{(r_{i-1} \cdot d_i) \times r_i}$ and $\mathcal{R} \in \mathbb{C}^{r_{i-1} \times (d_i \cdot r_i)}$ with $\mathcal{L}_{\overline{k,x},\ell} = \mathcal{R}_{k,\overline{x,\ell}} = T_{k,x,\ell}^{(i)}$. Here, the indices of two modes of $\mathbf{T}^{(i)}$ are lumped into

the multi-index $\overline{k, x}$ and $\overline{x, \ell}$, respectively, typically based on reverse lexicographic or colexicographic ordering. The remaining mode forms the other dimension of the unfolding matrix. We call the core $\mathbf{T}^{(i)}$ left-orthonormal if its left-unfolding is orthonormal with respect to the rows, i.e., $\mathcal{L}^\top \mathcal{L} = I \in \mathbb{R}^{r_i \times r_i}$. Correspondingly, a core is called right-orthonormal if its right-unfolding is orthonormal with respect to the columns, i.e., $\mathcal{R} \mathcal{R}^\top = I \in \mathbb{R}^{r_{i-1} \times r_{i-1}}$. In graphical notation, orthonormal components are depicted by half-filled circles, see Figure 3 (c).

In order to orthonormalize a given MPS with ranks (r_0, \dots, r_n) , we can apply a sequence of (truncated) SVDs to the cores of the decomposition. A right-orthonormal MPS representation, for example, can be obtained by iteratively computing the SVD $U\Sigma V^\top$ of the i th core and contracting the non-orthonormal part (i.e., $U\Sigma$) with the $(i-1)$ th core which is then decomposed in the next step. The (reshaped) matrix V^\top builds the updated core $\tilde{\mathbf{T}}^{(i)}$. Starting at the last MPS core $\mathbf{T}^{(n)}$ and repeating this procedure until reaching $\mathbf{T}^{(2)}$ results in a right-orthonormalized MPS decomposition $\tilde{\mathbf{T}}$ with cores $\tilde{\mathbf{T}}^{(i)} \in \mathbb{C}^{s_{i-1} \times d_i \times s_i}$ as required for the sampling technique described in Section 2.4. In fact, it holds that $\tilde{r}_i \leq r_i$ for $i = 0, \dots, n$, i.e., the ranks may become smaller while orthonormalizing if certain left- and right-unfoldings, respectively, exhibit a low-rank structure. Furthermore, truncated SVDs can be used to reduce the ranks by using absolute or relative cut-off criteria for the singular values, cf. [30]. In general, the computational complexity of left- and right-orthonormalizations, which are also known in the context of *Schmidt decompositions* of quantum systems, can be estimated as $O(ndr^3)$, where d denotes the maximum mode dimension and r the maximum rank of of \mathbf{T} .

A.1.3 Diagonal tensors as MPOs

Given a tensor $\mathbf{T} \in \mathbb{C}^{d_1 \times \dots \times d_n}$, we define the corresponding diagonal tensor $\text{diag}(\mathbf{T}) \in \mathbb{C}^{D \times D}$ by

$$\text{diag}(\mathbf{T})_{x_1, \dots, x_n, y_1, \dots, y_n} = \begin{cases} \mathbf{T}_{x_1, \dots, x_n}, & \text{if } x_i = y_i \text{ for } i = 1, \dots, n, \\ 0, & \text{otherwise.} \end{cases}$$

If \mathbf{T} is given as an MPS with cores $\mathbf{T}^{(i)} \in \mathbb{C}^{r_{i-1} \times d_i \times r_i}$, then $\text{diag}(\mathbf{T})$ can be written as an MPO with cores defined by

$$\text{diag}(\mathbf{T})_{k_{i-1}, x_i, y_i, k_i}^{(i)} = \begin{cases} \mathbf{T}_{k_{i-1}, x_i, k_i}^{(i)}, & \text{if } x_i = y_i, \\ 0, & \text{otherwise.} \end{cases}$$

Just as in standard linear algebra, it holds that $\text{diag}(\mathbf{T}) \cdot \mathbf{T} = \mathbf{T} \odot \mathbf{T}$, where \odot denotes the (multidimensional) Hadamard product.

A.2 MPO representations of quantum circuits

A.2.1 Quantum full adder

In order to derive the MPO representation (11), we consider the product (10) and concatenate the quantum gates successively. The product $\mathbf{G}_1 = \text{CNOT}(2 | 3) \cdot \text{CCNOT}(2, 3 | 4)$ is given by

$$\begin{aligned} \mathbf{G}_1 &= \left(I \otimes \begin{bmatrix} I & C \end{bmatrix} \otimes \begin{bmatrix} I & \\ \sigma_x - I & \end{bmatrix} \otimes I \right) \cdot \left(I \otimes \begin{bmatrix} I & C \end{bmatrix} \otimes \begin{bmatrix} I & 0 \\ 0 & C \end{bmatrix} \otimes \begin{bmatrix} I \\ \sigma_x - I \end{bmatrix} \right) \\ &= I \otimes \begin{bmatrix} I & C & C & C^2 \end{bmatrix} \otimes \begin{bmatrix} I & 0 \\ 0 & C \\ \sigma_x - I & 0 \\ 0 & (\sigma_x - I)C \end{bmatrix} \otimes \begin{bmatrix} I \\ \sigma_x - I \end{bmatrix}. \end{aligned}$$

Since $C^2 = C$, we can add the last three rows of the third core and get

$$\mathbf{G}_1 = I \otimes \begin{bmatrix} I & C \end{bmatrix} \otimes \begin{bmatrix} I & 0 \\ \sigma_x - I & \sigma_x C \end{bmatrix} \otimes \begin{bmatrix} I \\ \sigma_x - I \end{bmatrix}.$$

For the concatenation of the CNOT(3 | 1) and CCNOT(1, 3 | 4) gates, we have

$$\begin{aligned}
\mathbf{G}_2 &= \text{CNOT}(3 | 1) \cdot \text{CCNOT}(1, 3 | 4) \\
&= \left(\llbracket I \quad \sigma_x - I \rrbracket \otimes \llbracket I \quad 0 \rrbracket \otimes \llbracket I \rrbracket \otimes I \right) \cdot \left(\llbracket I \quad C \rrbracket \otimes \llbracket I \quad 0 \rrbracket \otimes \llbracket I \quad 0 \rrbracket \otimes \llbracket I \quad I \rrbracket \right) \\
&= \llbracket I \quad C \quad \sigma_x - I \quad (\sigma_x - I)C \rrbracket \otimes \begin{bmatrix} I & 0 & 0 & 0 \\ 0 & I & 0 & 0 \\ 0 & 0 & I & 0 \\ 0 & 0 & 0 & I \end{bmatrix} \otimes \begin{bmatrix} I & 0 \\ 0 & C \\ C & 0 \\ 0 & C \end{bmatrix} \otimes \llbracket I \\
&= \llbracket I \quad C \quad \sigma_x - I \quad (\sigma_x - I)C \rrbracket \otimes \begin{bmatrix} I & 0 & 0 \\ 0 & I & 0 \\ 0 & 0 & I \\ 0 & I & 0 \end{bmatrix} \otimes \begin{bmatrix} I & 0 \\ 0 & C \\ C & 0 \end{bmatrix} \otimes \llbracket I \\
&= \llbracket I \quad \sigma_x C \quad \sigma_x - I \rrbracket \otimes \begin{bmatrix} I & 0 & 0 \\ 0 & I & 0 \\ 0 & 0 & I \end{bmatrix} \otimes \begin{bmatrix} I & 0 \\ 0 & C \\ C & 0 \end{bmatrix} \otimes \llbracket I \quad \sigma_x - I \rrbracket.
\end{aligned}$$

In order to bring the first core into the desired form, cf. (11), we linearly combine the columns by multiplying with a (non-singular) matrix from the right. Therefore, we have to multiply the second core with the inverse of that matrix from the left to preserve the given MPO, i.e.,

$$\begin{aligned}
&\left(\llbracket I \quad \sigma_x C \quad \sigma_x - I \rrbracket \cdot \begin{bmatrix} 1 & 1 & 0 \\ -1 & 0 & 1 \\ 1 & 0 & 0 \end{bmatrix} \right) \otimes \left(\begin{bmatrix} 0 & 0 & 1 \\ 1 & 0 & -1 \\ 0 & 1 & 1 \end{bmatrix} \cdot \begin{bmatrix} I & 0 & 0 \\ 0 & I & 0 \\ 0 & 0 & I \end{bmatrix} \right) \\
&= \llbracket \sigma_x C_0 \quad I \quad \sigma_x C_1 \rrbracket \otimes \begin{bmatrix} 0 & 0 & I \\ I & 0 & -I \\ 0 & I & I \end{bmatrix},
\end{aligned}$$

where we use $C_0 = I - C$ and $C_1 = C$. Combining the above MPOs, we obtain

$$\begin{aligned}
\mathbf{G}_2 \cdot \mathbf{G}_1 &= \llbracket \sigma_x C_0 \quad I \quad \sigma_x C_1 \rrbracket \otimes \begin{bmatrix} 0 & 0 & 0 & 0 & I & C_1 \\ I & C_1 & 0 & 0 & -I & -C_1 \\ 0 & 0 & I & C_1 & I & C_1 \end{bmatrix} \\
&\otimes \begin{bmatrix} I & 0 & 0 & 0 \\ \sigma_x - I & \sigma_x C_1 & 0 & 0 \\ 0 & 0 & C_1 & 0 \\ 0 & 0 & C_1(\sigma_x - I) & C_1 \sigma_x C_1 \\ C_1 & 0 & 0 & 0 \\ C_1(\sigma_x - I) & C_1 \sigma_x C_1 & 0 & 0 \end{bmatrix} \otimes \begin{bmatrix} I \\ \sigma_x - I \\ \sigma_x - I \\ (\sigma_x - I)^2 \end{bmatrix}.
\end{aligned}$$

Since $C_1 \sigma_x C_1 = 0$, it follows that

$$\begin{aligned}
\mathbf{G}_2 \cdot \mathbf{G}_1 &= \llbracket \sigma_x C_0 \quad I \quad \sigma_x C_1 \rrbracket \otimes \begin{bmatrix} 0 & 0 & 0 & 0 & I & C_1 \\ I & C_1 & 0 & 0 & -I & -C_1 \\ 0 & 0 & I & C_1 & I & C_1 \end{bmatrix} \\
&\otimes \begin{bmatrix} I & 0 \\ \sigma_x - I & \sigma_x C_1 \\ 0 & C_1 \\ 0 & C_1(\sigma_x - I) \\ C_1 & 0 \\ C_1(\sigma_x - I) & 0 \end{bmatrix} \otimes \llbracket I \\
&\quad \quad \quad \otimes \llbracket \sigma_x - I \rrbracket.
\end{aligned}$$

Now, we manipulate the second core by

$$\begin{bmatrix} 0 & 0 & 0 & 0 & I & C_1 \\ I & C_1 & 0 & 0 & -I & -C_1 \\ 0 & 0 & I & C_1 & I & C_1 \end{bmatrix} \cdot \begin{bmatrix} 1 & 0 & 1 & 0 & 0 & 0 \\ -1 & 1 & -1 & 1 & 0 & 0 \\ -1 & 0 & 0 & 0 & 1 & 0 \\ 1 & -1 & 0 & 0 & -1 & 1 \\ 1 & 0 & 0 & 0 & 0 & 0 \\ -1 & 1 & 0 & 0 & 0 & 0 \end{bmatrix} = \begin{bmatrix} C_0 & C_1 & 0 & 0 & 0 & 0 \\ 0 & 0 & C_0 & C_1 & 0 & 0 \\ 0 & 0 & 0 & 0 & C_0 & C_1 \end{bmatrix},$$

and the last core by

$$\begin{bmatrix} 1 & 0 \\ 1 & 1 \end{bmatrix} \cdot \begin{bmatrix} I \\ \sigma_x - I \end{bmatrix} = \begin{bmatrix} I \\ \sigma_x \end{bmatrix}.$$

Thus, the third core becomes

$$\begin{bmatrix} 0 & 0 & 0 & 0 & 1 & 0 \\ 0 & 0 & 0 & 0 & 1 & 1 \\ 1 & 0 & 0 & 0 & -1 & 0 \\ 1 & 1 & 0 & 0 & -1 & -1 \\ 0 & 0 & 1 & 0 & 1 & 0 \\ 0 & 0 & 1 & 1 & 1 & 1 \end{bmatrix} \cdot \begin{bmatrix} I & 0 \\ \sigma_x - I & \sigma_x C_1 \\ 0 & C_1 \\ 0 & C_1(\sigma_x - I) \\ C_1 & 0 \\ C_1(\sigma_x - I) & 0 \end{bmatrix} \cdot \begin{bmatrix} 1 & 0 \\ -1 & 1 \end{bmatrix} = \begin{bmatrix} C_1 & 0 \\ C_1 \sigma_x & 0 \\ C_0 & 0 \\ 0 & \sigma_x C_1 \\ 0 & C_1 \\ 0 & C_1 \sigma_x \end{bmatrix}.$$

Thus, we can express the MPO operator \mathbf{G} (10) as the product

$$\mathbf{G} = \text{CNOT}(2 | 3) \cdot \mathbf{G}_2 \cdot \mathbf{G}_1 = \left(I \otimes \begin{bmatrix} C_0 & C_1 \end{bmatrix} \otimes \begin{bmatrix} I \\ \sigma_x \end{bmatrix} \otimes I \right) \cdot \mathbf{G}_2 \cdot \mathbf{G}_1.$$

Since the first and last core of $\text{CNOT}(2 | 3)$ are simply given by the identity matrix, let us only consider the second and third core of the product. We obtain

$$\begin{aligned} \begin{bmatrix} \mathbf{G}^{(2)} \end{bmatrix} \otimes \begin{bmatrix} \mathbf{G}^{(3)} \end{bmatrix} &= \begin{bmatrix} C_0 & 0 & 0 & 0 & 0 & 0 & 0 & 0 & C_1 & 0 & 0 & 0 & 0 \\ 0 & 0 & C_0 & 0 & 0 & 0 & 0 & 0 & 0 & 0 & C_1 & 0 & 0 \\ 0 & 0 & 0 & 0 & C_0 & 0 & 0 & 0 & 0 & 0 & 0 & 0 & C_1 \end{bmatrix} \otimes \begin{bmatrix} C_1 & 0 \\ C_1 \sigma_x & 0 \\ C_0 & 0 \\ 0 & \sigma_x C_1 \\ 0 & C_1 \\ 0 & C_1 \sigma_x \\ \sigma_x C_1 & 0 \\ C_0 & 0 \\ \sigma_x C_0 & 0 \\ 0 & C_1 \\ 0 & \sigma_x C_1 \\ 0 & C_0 \end{bmatrix} \\ &= \begin{bmatrix} C_0 & C_1 & 0 & 0 \\ 0 & C_0 & C_1 & 0 \\ 0 & 0 & C_0 & C_1 \end{bmatrix} \otimes \begin{bmatrix} C_1 & 0 \\ C_0 & 0 \\ 0 & C_1 \\ 0 & C_0 \end{bmatrix}, \end{aligned}$$

which leads to the decomposition (11).

A.2.2 Simon's algorithm

We have

$$\mathbf{G}_1 = \mathbf{G}_4 = H \otimes I \otimes H \otimes I \otimes H \otimes I \otimes H \otimes I.$$

Furthermore, it holds that

$$\begin{aligned} \mathbf{G}_3 &= \begin{bmatrix} I & C \end{bmatrix} \otimes \begin{bmatrix} I \\ I \end{bmatrix} \otimes \begin{bmatrix} I \\ I \end{bmatrix} \otimes \begin{bmatrix} I \\ I \end{bmatrix} \otimes \begin{bmatrix} I \\ I \end{bmatrix} \otimes \begin{bmatrix} I \\ I \end{bmatrix} \otimes \begin{bmatrix} I \\ \sigma_x - I \end{bmatrix} \otimes I \otimes I \\ &\cdot \begin{bmatrix} I & C \end{bmatrix} \otimes \begin{bmatrix} I \\ \sigma_x - I \end{bmatrix} \otimes I \otimes I \otimes I \otimes I \otimes I \otimes I \otimes I, \end{aligned}$$

which can be rewritten as

$$\begin{aligned}
\mathbf{G}_3 &= \begin{bmatrix} C_0 & C_1 \end{bmatrix} \otimes \begin{bmatrix} I & \\ & I \end{bmatrix} \otimes \begin{bmatrix} I & \\ & I \end{bmatrix} \otimes \begin{bmatrix} I & \\ & I \end{bmatrix} \otimes \begin{bmatrix} I & \\ & I \end{bmatrix} \otimes \begin{bmatrix} I \\ \sigma_x \end{bmatrix} \otimes I \otimes I \\
&\cdot \begin{bmatrix} C_0 & C_1 \end{bmatrix} \otimes \begin{bmatrix} I \\ \sigma_x \end{bmatrix} \otimes I \otimes I \otimes I \otimes I \otimes I \otimes I \\
&= \begin{bmatrix} C_0 & C_1 \end{bmatrix} \otimes \begin{bmatrix} I & \\ & \sigma_x \end{bmatrix} \otimes \begin{bmatrix} I & \\ & I \end{bmatrix} \otimes \begin{bmatrix} I & \\ & I \end{bmatrix} \otimes \begin{bmatrix} I & \\ & I \end{bmatrix} \otimes \begin{bmatrix} I \\ \sigma_x \end{bmatrix} \otimes I \otimes I,
\end{aligned}$$

see Example 2. The product of \mathbf{G}_3 and \mathbf{G}_2 (see Section 3.2) can then be expressed as

$$\begin{aligned}
\mathbf{G}_3 \cdot \mathbf{G}_2 &= \begin{bmatrix} C_0 & C_1 \end{bmatrix} \otimes \begin{bmatrix} I & \\ & I \end{bmatrix} \otimes \begin{bmatrix} C_0 & C_1 & C_0 & C_1 \end{bmatrix} \otimes \begin{bmatrix} I & \\ \sigma_x & \\ & I \end{bmatrix} \\
&\otimes \begin{bmatrix} C_0 & C_1 \\ C_1 & C_0 \end{bmatrix} \otimes \begin{bmatrix} I \\ \sigma_x \end{bmatrix} \otimes \begin{bmatrix} C_0 & C_1 \end{bmatrix} \otimes \begin{bmatrix} I \\ \sigma_x \end{bmatrix}.
\end{aligned}$$

Multiplying the cores with odd indices by H from left and right results in the MPO (13).

A.2.3 Quantum Fourier transform

As already mentioned in Section 2.2, we can swap the roles of the control and target qubit for a controlled phase-shift gate. That is, by repeatedly applying (18), we have

$$\begin{aligned}
\text{CPHASE}_k(p | q) &= I^{\otimes(p-1)} \otimes \begin{bmatrix} C_0 & C_1 \end{bmatrix} \otimes \begin{bmatrix} I^{\otimes(q-p-1)} & \\ & I^{\otimes(q-p-1)} \end{bmatrix} \otimes \begin{bmatrix} I \\ R_k \end{bmatrix} \otimes I^{\otimes(n-q)} \\
&= I^{\otimes(p-1)} \otimes \begin{bmatrix} C_0 & C_1 \end{bmatrix} \otimes \begin{bmatrix} I^{\otimes(q-p-1)} & \\ & I^{\otimes(q-p-1)} \end{bmatrix} \\
&\quad \otimes \left(\begin{bmatrix} 1 & 1 \\ 1 & e^{\frac{2\pi i}{k}} \end{bmatrix} \cdot \begin{bmatrix} C_0 \\ C_1 \end{bmatrix} \right) \otimes I^{\otimes(n-q)} \\
&= I^{\otimes(p-1)} \otimes \left(\begin{bmatrix} C_0 & C_1 \end{bmatrix} \cdot \begin{bmatrix} 1 & 1 \\ 1 & e^{\frac{2\pi i}{k}} \end{bmatrix} \right) \otimes \begin{bmatrix} I^{\otimes(q-p-1)} & \\ & I^{\otimes(q-p-1)} \end{bmatrix} \\
&\quad \otimes \begin{bmatrix} C_0 \\ C_1 \end{bmatrix} \otimes I^{\otimes(n-q)} \\
&= I^{\otimes(p-1)} \otimes \begin{bmatrix} I & R_k \end{bmatrix} \otimes \begin{bmatrix} I^{\otimes(q-p-1)} & \\ & I^{\otimes(q-p-1)} \end{bmatrix} \otimes \begin{bmatrix} C_0 \\ C_1 \end{bmatrix} \otimes I^{\otimes(n-q)} \\
&= \text{CPHASE}_k(q | p),
\end{aligned}$$

where $\text{CPHASE}_k(p | q)$ denotes a controlled phase-shift gate as described in Section 3.3, which applies R_k to the target qubit q if the control qubit p is in state $|1\rangle$. Thus, each gate group \mathbf{G}_i , $i = 1, \dots, n-1$, of the QFT can be written as

$$\begin{aligned}
\mathbf{G}_i &= \text{CPHASE}_{n-i+1}(n, i) \cdots \text{CPHASE}_2(i+1, i) \cdot \left(I^{\otimes(i-1)} \otimes H \otimes I^{\otimes(n-i)} \right) \\
&= \text{CPHASE}_{n-i+1}(i, n) \cdots \text{CPHASE}_2(i, i+1) \cdot \left(I^{\otimes(i-1)} \otimes H \otimes I^{\otimes(n-i)} \right) \\
&= \left(I^{\otimes(i-1)} \otimes \begin{bmatrix} C_0 & C_1 \end{bmatrix} \otimes \begin{bmatrix} I & \\ & R_2 \end{bmatrix} \otimes \cdots \otimes \begin{bmatrix} I & \\ & R_{n-i+1} \end{bmatrix} \right) \cdot \left(I^{\otimes(i-1)} \otimes H \otimes I^{\otimes(n-i)} \right) \\
&= \frac{1}{\sqrt{2}} I^{\otimes(i-1)} \otimes \begin{bmatrix} 1 & 1 \\ 0 & 0 \end{bmatrix} \begin{bmatrix} 0 & 0 \\ 1 & -1 \end{bmatrix} \otimes \begin{bmatrix} I & \\ & R_2 \end{bmatrix} \otimes \cdots \otimes \begin{bmatrix} I & \\ & R_{n-i} \end{bmatrix} \otimes \begin{bmatrix} I \\ R_{n-i+1} \end{bmatrix}.
\end{aligned}$$

The MPO representation of the inverse QFT can be derived analogously.